https://doi.org/10.5194/egusphere-2026-3617
Preprint. Discussion started: 30 June 2026

A Phanerozoic-style icehouse climate in the middle Ediacaran

Thomas W. Wong Hearing[1], Alexandre Pohl[2], Thomas M. Vandyk[1], Benjamin H. Tindal[3], Frédéric Fluteau[4], Alexander G. Liu[5], Thomas H. P. Harvey[1], Mark Williams[1]

[1]Centre for Palaeobiology and Biosphere Evolution, School of Geography, Geology and the Environment, University of Leicester, Leicester, LE1 7RH, UK.
[2]Université Bourgogne Europe, CNRS, Biogéosciences UMR 6282, 21000 Dijon, France.
[3]Chief Scientist's Directorate, Natural England, 8 City Walk, Leeds, LS11 9AT, UK.
[4]Université Paris Cité, Institut de physique du globe de Paris, CNRS, 1 Rue Jussieu, F-75005, Paris, France
[5]Department of Earth Sciences, Downing Street, University of Cambridge, Cambridge, CB2 3EQ, UK.
Correspondence to: Thomas W. Wong Hearing(twonghearing@gmail.com); Alexandre Pohl (alexandre.pohl@cnrs.fr); Thomas H. P. Harvey (thph2@le.ac.uk); Mark Williams (mri@le.ac.uk)

Abstract. Geological evidence points to icehouse conditions during the Ediacaran Period (635 to 538.8 Ma) both before and during the emergence of animals in the fossil record. However, the temporal and spatial distributions of Ediacaran ice sheets are not well constrained due to uncertainties in palaeogeography, chronostratigraphy, and the depositional settings of candidate glaciogenic deposits. Here, we systematically evaluate the evidence for the depositional ages of candidate Ediacaran glaciogenic deposits and establish the likelihood that each deposit was formed by ice-driven processes using observation-driven weighting criteria. Our analysis supports the existence of discrete mid- and late Ediacaran icehouse intervals (MEIH and LEIH respectively), each followed by greenhouse conditions. Focussing on the older MEIH, we integrate our quality-controlled geological dataset with climate and ice sheet model simulations to characterise glacial conditions during this interval (~593 to 579 Ma), which encompasses the 'Gaskiers glaciation'. Our results indicate that the MEIH was a Phanerozoic-style icehouse, with latitudinally-constrained and fluctuating ice sheets, marking a break from the preceding Cryogenian snowball Earth motif, and occurring before the first known appearance of animals in the fossil record. By mapping robustly identified glaciogenic deposits onto contrasting middle Ediacaran palaeogeographic reconstructions, we show how these deposits can be used to constrain hypotheses of Ediacaran continental configuration.

1 Introduction

1.1 Icehouse intervals in Earth history

Throughout the Phanerozoic Eon (~538.8 Ma to present), Earth's climate has alternated between two primary states, icehouse and greenhouse (e.g. Fischer, 1981; Judd et al., 2024; Macdonald et al., 2019; Scotese et al., 2021; Umbgrove, 1947; Westerhold et al., 2020). To a first approximation, conditions during the various Phanerozoic icehouse intervals were remarkably consistent in terms of global mean surface temperatures (Judd et al., 2024; Scotese et al., 2021; Westerhold et al., 2020) and the maximum latitudinal extent of low-altitude ice sheets (Evans, 2003; Macdonald et al., 2019; Merdith et al.,

https://doi.org/10.5194/egusphere-2026-3617
Preprint. Discussion started: 30 June 2026

2025). Coupled climate-ice sheet model simulations suggest that the land-ice front readily advances to ~40 ° latitude, but feedbacks between ice sheets and global climate cause the ice line to stabilise at these latitudes, and the steep temperature gradient towards the equator makes further ice advance much more challenging to achieve (Pohl et al., 2016a).

However, this pattern does not hold for earlier icehouse intervals in Earth's history (Hoffman et al., 1998, 2017; Kirschvink, 1992). Rocks deposited during the Neoproterozoic Cryogenian Period (~720 to 635 Ma) contain evidence that has been interpreted as recording two episodes of extreme 'snowball Earth' glaciation, with global or near-global ice coverage (Evans, 2003; Hoffman et al., 1998, 2017; Kirschvink, 1992). Simple energy balance models and some more complex general circulation models suggest that feedbacks in the climate system render a snowball-style glaciation inevitable once the ice line reaches tropical latitudes (e.g. Budyko, 1969; Hoffman et al., 2017; Tasistro-Hart et al., 2025). The Cryogenian and Phanerozoic therefore present two distinct modes of icehouse climate state on Earth (Table 1), and the change between these modes has been implicated in the emergence of animals during the Ediacaran Period (~635 to 538.8 Ma) (e.g. Evans, 2003).

The Ediacaran Period was a transformational interval for the Earth system bridging the Proterozoic and Phanerozoic worlds, and witnessed the emergence of marine ecosystems with complex macroscopic organisms including animals (Boag et al., 2024; Matthews et al., 2021; Pu et al., 2016; Rooney et al., 2020; Xiao and Narbonne, 2020; Yang et al., 2021; Yuan et al., 2011). Resolving the nature of Ediacaran climate is thus crucial to understanding the primary controls on Earth's climate system, the timing of the transition from 'snowball Earth' to Phanerozoic-type climate states, and the interplay of the physical Earth system with biotic innovations through this interval (Wong Hearing et al., 2026). In this study, we set out to test climate and ice sheet model simulations against the geological record of mid-Ediacaran glacial ice to provide a robust first-order constraint on the nature of the Ediacaran climate system.

Table 1. A summary of Neoproterozoic and Phanerozoic icehouse climate intervals. See Data S2.

Name	Duration	Lowest latitude of low altitude ice sheets	References
Late Cenozoic icehouse	Eocene-Oligocene transition to present day (~34 to 0 Ma)	~40°	Macdonald et al. (2019)
Late Palaeozoic Ice Age (LPIA)	Middle Mississippian to Guadalupian (~340 to 260 Ma)	~40°	Macdonald et al. (2019)
Late Devonian icehouse (the early part of or a prelude to the LPIA)	Famennian (~365 to 357 Ma)	~70°	Macdonald et al. (2019)
Early Palaeozoic icehouse	Ordovician to Silurian (~460 to 420 Ma)	~40°	Macdonald et al. (2019)
Late Ediacaran icehouse (LEIH)	Late Ediacaran (~565 or 560 to 550 Ma)	Uncertain; not global	Wong Hearing et al. (2026) and this study
Mid-Ediacaran icehouse (MEIH)	Mid-Ediacaran (~593 to 579 Ma)	~40° (PALEOMAP); ~30° (MERDITH2021)	This study
Marinoan icehouse	Late Cryogenian (650 or 639 to 635 Ma)	Global?	Hoffman et al. (2017); Tasistro-Hart et al. (2025)
Sturtian icehouse	Early to mid-Cryogenian (717 to 659 Ma)	Global?	Hoffman et al. (2017); Tasistro-Hart et al. (2025)

https://doi.org/10.5194/egusphere-2026-3617
Preprint. Discussion started: 30 June 2026

1.2 Icehouse conditions in the Ediacaran Period

There is strong evidence for at least one, and possibly up to four, major glaciations during the Ediacaran Period (Chumakov, 2009; Linnemann et al., 2018, 2022; Liu et al., 2025; Niu et al., 2024; Pu et al., 2016; Retallack, 2022; Wang et al., 2023a, b; Wong Hearing et al., 2026; Youbi et al., 2020). Confusion has developed in the published literature regarding the number and temporal distribution of candidate Ediacaran glaciogenic deposits and, therefore, of glacial episodes, largely because of a lack of consideration of the geological constraints on the depositional age and formation conditions of these deposits (Wong Hearing et al., 2026). In particular, two schools of thought have developed: one which interprets the record as reflecting a series of discrete glacial episodes (Linnemann et al., 2018, 2022; Niu et al., 2024; Retallack, 2022; Youbi et al., 2020), and one which interprets the record as reflecting a single 20 to 40 million year 'great late Ediacaran ice age' (Liu et al., 2025; Wang et al., 2023a, b). An extraordinary palaeogeographic hypothesis of inertial interchange true polar wander has been invoked to explain the distribution of candidate glacial deposits under the great late Ediacaran ice age model (Wang et al., 2023a).

Our previous work, updated here (Fig. 1), evaluated the likelihood that candidate mid- to late Ediacaran glaciogenic deposits were in fact mid- to late Ediacaran in age and glacial in origin (Wong Hearing et al., 2026). We found that careful consideration of the evidence for both depositional age and environment indicates that there were most likely two icehouse intervals and two greenhouse intervals in the mid- to late Ediacaran (Fig. 1), which correspond with distinct biotic assemblages in the fossil record (Wong Hearing et al., 2026). In particular, we found that there was an absence of well-constrained glaciogenic deposits between 579 to 565 Ma, including in regions that have positive evidence of well-constrained glaciogenic deposits before and after this interval, supporting two distinct icehouse climate states: the 'mid-Ediacaran icehouse' (MEIH) and the 'late Ediacaran icehouse' (LEIH) (Wong Hearing et al., 2026).

1.3 The 'mid-Ediacaran icehouse' (MEIH)

In this study we focus on constraining the timing, palaeogeographic extent, and climatic characteristics of the first of the glacial intervals, the 'mid-Ediacaran icehouse'. The MEIH has primarily been associated with deposits of the Gaskiers Formation and the Trinity diamictite of eastern Newfoundland, Canada, which were interpreted as recording a short-lived glaciation (possibly as little as 1 Myr duration; Pu et al., 2016) of uncertain geographical extent. However, recently discovered field evidence suggests that these iconic deposits represent the final phase of a more protracted cold interval on Avalonia (Fitzgerald et al., 2024; Gómez et al., 2025a, b, 2026; Mills et al., 2024). Underlying the Gaskiers Formation, rocks of the Mall Bay Formation were deposited proximal to sea level freezing conditions for perhaps the preceding 5 Myr (Fitzgerald et al., 2024). Recent radiometric dating and sedimentological work on the Rocky Harbour Group, containing the Trinity and Mercantile diamictites, also suggest that glacial conditions existed on Avalonia between ~589 to 579 Ma (Gómez et al., 2025a, b, 2026; Mills et al., 2024). Additional candidate glaciogenic deposits generally correlated with the Gaskiers Formation (Carto and Eyles, 2011; Letsch et al., 2018; Linnemann et al., 2018; Niu et al., 2024; Pecoits et al., 2011; Thompson and Bowring, 2000; Youbi et al., 2020) further support a longer duration icehouse interval terminating at ~579 Ma (Fig. 1).

https://doi.org/10.5194/egusphere-2026-3617
Preprint. Discussion started: 30 June 2026

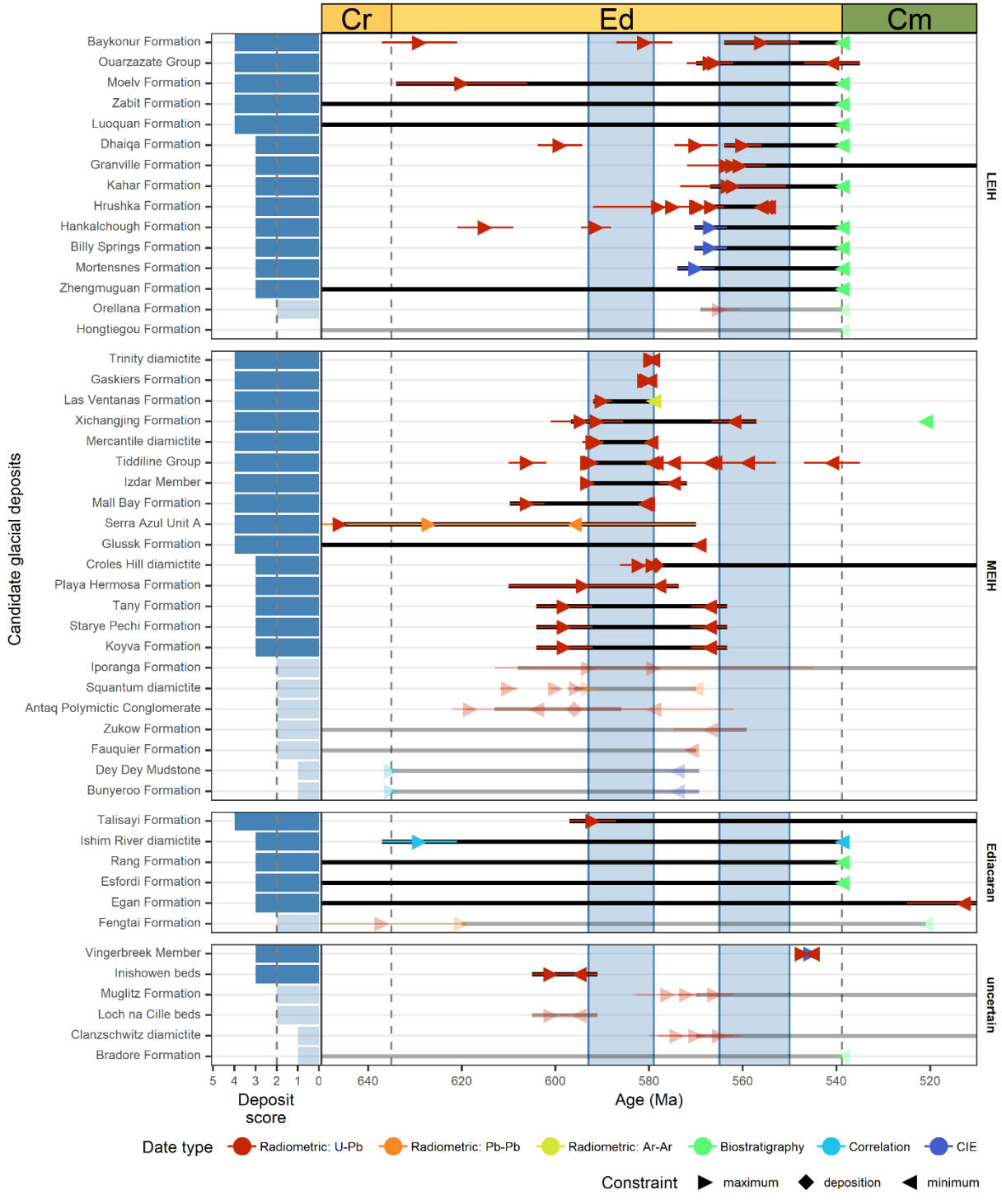

https://doi.org/10.5194/egusphere-2026-3617
Preprint. Discussion started: 30 June 2026

Fig. 1. Temporal distribution of Ediacaran candidate glaciogenic deposits and their likelihood (deposit score) of having a glacial origin. Deposits arranged by likely interval: MEIH = mid-Ediacaran icehouse, ~593 to 579 Ma; LEIH = late Ediacaran icehouse, ~565 to 550 Ma; "Ediacaran" deposits are constrained only to the Ediacaran Period; "uncertain" deposits may be Ediacaran in age but have unreliable or disputed age constraints (see Supplementary Information). Deposits scoring less than three stars (less than circumstantial) are faded out. Thick solid lines show the maximum permitted range for each deposit, including analytical uncertainty where relevant. Symbols show the type of constraint, i.e. whether the date provides a minimum, maximum, or depositional age for a deposit. Vertical blue regions show the likely intervals of the MEIH and LEIH. CIE: carbon isotope excursion; Cr: Cryogenian (pars.); Ed: Ediacaran; Cm: Cambrian (pars.). See Wong Hearing et al. (2026).

1.4 Palaeogeography and modelling Ediacaran climate

In contrast to the preceding Cryogenian, there have been few attempts to use numerical models to simulate Ediacaran climate (e.g. Goddéris et al., 2007; Liu et al., 2025). This is likely to reflect uncertainty in reconstructing palaeogeography during this period, which is a required boundary condition for general circulation models. A disparate range of palaeogeographic hypotheses have been suggested for the Ediacaran (e.g. Domeier et al., 2023; Merdith et al., 2021; Scotese, 2016; Scotese and Wright, 2018; Wen et al., 2022), and Ediacaran palaeogeography remains uncertain in part because palaeomagnetic data from this interval are very difficult to interpret (Domeier et al., 2023). Possible explanations include remagnetisation, anomalous magnetic field behaviour, anomalously high rates of plate motion, or one or more intervals of inertial interchange true polar wander (TPW) in which Earth's continents rapidly reorientated relative to its rotation and magnetic field axes (Domeier et al., 2023).

Late Ediacaran redistribution of the continents due to TPW (Wen et al., 2022) has been invoked to support the hypothesis of a 'great late Ediacaran ice age' (Liu et al., 2025; Wang et al., 2023a, b). In particular, a recent modelling study set out to test whether the 'great late Ediacaran ice age' could be sustained over most of the late Ediacaran interval (~580 to <560 Ma) and explain the observed distribution of glacial deposits using a TPW-derived palaeogeographic configuration (Liu et al., 2025). Liu et al. (2025) concluded that aligning their data compilation with their model results required very low atmospheric partial pressures of CO_2 (pCO_2) ranging between 35 and 280 ppmv (0.125 to 1 times pre-industrial atmospheric levels [PAL]). The simulated climates were very cold, with global mean surface temperatures of –4.2 to +1.6 °C, and were characterised by sea ice cover extending into the subtropics. Any further equatorward extension of the sea ice line would likely trigger a pan-glacial snowball state (Bendtsen, 2002; Budyko, 1969; Hoffman et al., 2017). These results suggest that only a narrow range of atmospheric CO_2 concentrations could allow a mid-Ediacaran ice sheet to align with the sedimentological evidence while avoiding global glaciation. This inference calls into question the geological stability, and therefore plausibility, of Phanerozoic-like, non-snowball, icehouse conditions during the mid-Ediacaran.

Here, we test whether palaeogeographic configurations not derived from hypotheses of a TPW event can find agreement between rigorously vetted geological data and model simulations of Ediacaran climate. We explicitly consider two possible continental configurations for the mid-Ediacaran: PALEOMAP (Scotese, 2016; Scotese and Wright, 2018) and MERDITH2021 (Merdith et al., 2021). These configurations are widely used in deep time climate and palaeobiology studies, and have the advantage of belonging to series of internally consistent rotation models that span the Neoproterozoic–Phanerozoic transition, ensuring that models are reconciled with the better constrained positions of continents in the early

https://doi.org/10.5194/egusphere-2026-3617
Preprint. Discussion started: 30 June 2026

Phanerozoic. We also draw comparisons between our results using the PALEOMAP and MERDITH2021 configurations, and those derived from a TPW palaeogeography (Liu et al., 2025; Wang et al., 2023a, b). Our analyses enable us to constrain the nature of the icehouse mode Earth's climate system was operating under immediately prior to the emergence of animal-rich marine ecosystems in the late Ediacaran (from ~575 Ma; Boag et al., 2024; Matthews et al., 2021).

2 Methods

2.1 Geological data

The glaciogenic sedimentary record provides the best constraint on first-order climate state for the Ediacaran because of the absence of robust and widespread palaeo-temperature proxies for this interval (e.g. Evans, 2003; Evans and Raub, 2011; Macdonald et al., 2019; Merdith et al., 2025). However, inconsistencies and uncertainties in the identification of candidate glaciogenic deposits have hampered our understanding of the Ediacaran glaciogenic sedimentary record because previous studies have not provided systematic and reproducible criteria for including or excluding specific deposits (Wong Hearing et al., 2026). To tackle this, we compiled a dataset of candidate mid- and late Ediacaran glaciogenic deposits following Wong Hearing et al. (2026). Our dataset considers all deposits included in recent compilations of candidate Ediacaran glaciogenic deposits (Niu et al., 2024; Retallack, 2022; Wang et al., 2023a, b; Youbi et al., 2020) and additional data drawn from literature searches. The full dataset is presented in Data S1.

For each deposit, we first assessed the depositional age constraints (see below). Deposits with a plausibly mid-Ediacaran depositional age were further assessed for the likelihood that they were glacial in origin (see below). Detailed glaciogenicity assessments of the candidate mid-Ediacaran glaciogenic deposits are provided in the Supplementary Information.

2.2 Assessing depositional age

Radiometric date constraints are the preferred means of depositional age control, with chemical abrasion isotope dilution thermal ionisation mass spectrometry (CA-ID-TIMS) U-Pb dates from igneous zircons considered the most informative. Detrital zircon and shale Re-Os dates are also used to establish maximum and depositional age constraints, respectively. We include the reported analytical uncertainty of radiometric dates in our analysis. Where relevant, Phanerozoic fossils are used to indicate that the host deposit is younger than 538.8 Ma (the current age of the Ediacaran–Cambrian boundary following the International Commission on Stratigraphy; Cohen et al., 2025), or to provide a more specific age where possible. Note that the numeric age of the Ediacaran–Cambrian boundary (currently 538.8 Ma) is less significant in this case than is the recognition of the stratigraphic boundary itself, and that the numeric age is likely to change in the near future (Bowyer and Nelson, 2026). Where Ediacaran fossils are found overlying a candidate glaciogenic deposit, we consider these to provide a minimum depositional age constraint of 538.8 Ma, i.e. deposition before the end of the Ediacaran Period, although we only use Ediacaran palaeontological constraints when radiometric ages are unavailable. Carbon isotope stratigraphy is used only in the case of the

https://doi.org/10.5194/egusphere-2026-3617
Preprint. Discussion started: 30 June 2026

Shuram carbon isotope excursion which has a distinctive profile and is dated to ~574 to 567 Ma (Busch et al., 2023; Rooney et al., 2020; Yang et al., 2021).

2.3 Assessing glaciogenicity

We follow the glaciogenicity rating scheme originally devised by Tindal (2023) and applied by Wong Hearing et al. (2026), updated here to better account for broader depositional context (see Supplementary Information). The deposit scoring scheme accounts for the wide variety of sedimentological and depositional evidence for glaciogenicity observed in the rock record (Table 2), much of which can also result from non-glacial processes. The scheme is summarised in Table 2 and Table 3, and is described in detail in the Supplementary Information, including the specific sedimentological characteristics used to assign star ratings, with an overview provided here.

The deposit scoring scheme combines multiple individual lines of sedimentological evidence, including overall rock texture, clast shape, angularity or roundness, surface features, lithology, geomorphology, and depositional context. Under this additive scheme, multiple lines of weaker evidence co-occurring within a single deposit contribute to a stronger overall score for the likely glaciogenicity of the deposit as a whole. This overall deposit score is derived from the geometric progression (interval ratio ½) combining multiple lines of evidence (Table 3); that is, a one-star line of evidence is worth half that of a two-star line of evidence, and similarly a one-star deposit score is worth half the value of a two-star deposit score (Tindal, 2023). The overall rating for a deposit is calculated from the weighted sum of the different reported lines of evidence. In this way, we can apply the semi-quantitative scheme consistently across deposits with different degrees of information, and ratings can be readily updated as new information comes to light.

This rating scheme does not guarantee the glaciogenicity or lack thereof for any deposit, as it seeks to quantify a range of qualitative data and necessarily loses some of the nuance essential to any holistic sedimentological study. It provides a systematic approach for assessing potential glaciogenicity throughout the geological record, but should only be considered a guide to support the interpretation of candidate glaciogenic deposits (Wong Hearing et al., 2026). Following Tindal (2023) and Wong Hearing et al. (2026), we suggest that deposits meeting a specific threshold should be regarded as plausibly glaciogenic, while those falling below the threshold are either unlikely to be glaciogenic, or have not been described in sufficient detail to support a confident glaciogenic interpretation.

Applying a threshold requires striking a balance between minimising false positives (deposits erroneously interpreted as glaciogenic on the basis of insufficient evidence) and false negatives (truly glaciogenic deposits with either relatively weak sedimentological evidence, or inadequately described for assessment). We adopt a three-star score (= “circumstantial”; Table 3) as a suitable minimum threshold for a deposit being plausibly glaciogenic and worthy of further consideration. The three-star threshold will still include deposits that may be considered unlikely to be glaciogenic on the basis of other evidence, and three-star deposits in particular should be inspected on a case-by-case basis.

https://doi.org/10.5194/egusphere-2026-3617
Preprint. Discussion started: 30 June 2026

185 **Table 2. Summary of the sedimentary and geomorphological evidence used in Tindal's (2023) deposit scoring scheme. Adapted from Tindal (2023, table 2.1 to 2.11) and Wong Hearing et al. (2026, table 2). For a full description and an explanation of the evidence categories and ranking see Tindal (2023, chapter 2).**

	Star rating of each line of evidence				
Evidence category	★★★★★	★★★★	★★★	★★	★
Clast-rich diamictite	–	–	Outsized clasts deposited as a massive or stratified diamictite in a flat or distal setting not on or near the base of a slope.	–	Outsized clasts deposited as a massive or stratified diamictite in a setting with other reworked deposits.
Clast-poor diamictite	–	–	Outsized clasts that: (i) disrupt laminae above/below in a flat or distal setting not on or near the base of a slope; or (ii) are deposited as a massive or stratified diamictite in a flat or distal setting not on or near the base of a slope.	Outsized clasts that disrupt laminae above/below, from a setting where downslope transport is not reported, or confirmed absent.	Outsized clasts that may disrupt laminae above/below in or associated with reworked deposits.
Clast shape	–	–	–	Several elongate or fragile clasts.	Clasts from at least four of Powers (1953) grades of roundness, including subangular and subrounded, or a few elongate clasts.
Clast surfaces	–	–	Clasts with striated and facetted surfaces.	–	Clasts with either facetted surfaces or striae.
Clast lithologies	–	–	Clasts include all of siliciclastic, carbonate, metamorphic, and igneous lithologies; or lithologies not otherwise known from the basin; or non-abraded clasts (i.e. little physical weathering) that must have travelled at least 100 km.	Clasts include three of siliciclastic, carbonate, metamorphic, and igneous lithologies.	Clasts include two of siliciclastic, carbonate, metamorphic, and igneous lithologies; or diamictite described as "heterogeneous" or "polymict" without further description.

https://doi.org/10.5194/egusphere-2026-3617
Preprint. Discussion started: 30 June 2026

Grain clusters	–	Uncemented clusters of close-packed interlocking outsized grains, isolated in a fine-grained sediment without evidence of current flow, disrupting laminae (if present), and occurring at multiple closely spaced stratigraphic horizons.	Uncemented clusters of close-packed interlocking outsized grains, isolated in a fine-grained sediment without evidence of current flow and disrupting laminae (if present).	Uncemented clusters of outsized granules in a fine-grained matrix that may host other sediment grains without specific evidence of current flow for their deposition though surrounding sediment may show signs of current flow for deposition.	Uncemented clusters of outsized clasts without evidence of erosive lower contacts.
Surface striation	Extensive striated surfaces with crescentic gouges, chattermarks and s-forms.	Extensive surfaces with striae and some but not all of the features listed for a five.	Extensive surfaces with striae and/or small surfaces with features listed above	Large smooth surfaces and/or small surfaces with striae	Small smooth surfaces
Geo-morphological forms	–	–	U-shaped valleys or branching valley networks	Roche moutonneé-like palaeotopography, moraine-like ridges	–
Glacio-tectonism	–	Extensive surfaces of parallel grooves showing multiple phases of scraping	>10 m scale cylindrical folding of beds with undeformed underlying beds	Cylindrical folding of beds with undeformed underlying beds	Deformed beds with undeformed underlying beds
Soft sediment ploughing (keel drag)	–	–	Extensive surfaces of parallel grooves	Small surfaces of parallel grooves	Deformed beds
Frost polygons	–	Extensive areas of large polygons with infilled wedges deeper than 20 cm	Extensive areas of large polygons of wedges infilled with coarse material	Large polygonal cracks	Infilled wedges deeper than 20 cm
Cryoturbation	–	–	Extensive (>1 km2) areas of deformed sediment with rigidly deformed layers and oriented stones	Deformed sediment described as cryoturbation with rigidly deformed layers and/or oriented stones	–
Casts of ice crystals	–	Blade-shaped imprints of ice crystals	Imprints of ice crystals (no further description)	–	–
Shattered clasts	–	–	*In situ* clast, fractured into multiple pieces on subaerial substrate	In situ clast, fractured into multiple pieces	Angular clasts of the same lithology in close proximity

https://doi.org/10.5194/egusphere-2026-3617
Preprint. Discussion started: 30 June 2026

Varves	–	–	–	Rhythmically spaced parallel laminations of alternating composition	Parallel laminations of alternating composition

Table 3. Summary of the overall deposit score (zero to five stars) system presented in the figures and analysis used here, adapted from Tindal (2023, tbl. 2.1) and Wong Hearing et al. (2026, tbl. 3). See Supplementary Information for a full discussion on rating glaciogenic deposits under this scheme.

Strength	Deposit score	Relative weight[a]	Example deposit
Unequivocal	★★★★★	1	NA[b]
Strong	★★★★	1/2	Gaskiers Formation: diamictite and dropstones (★) with very angular to well-rounded clasts (★) from 3 lithological groups (★★), some of which are facetted or striated (★★★).
Circumstantial	★★★	1/4	Granville Formation: diamictite with rounded to well-rounded clasts from three lithological groups (★★), some of which are striated (★★★).
Weak	★★	1/8	Orellana Formation: diamictite and dropstones (★) with clasts of unreported roundness from one lithological group, some of which are facetted (★).
Equivocal	★	1/16	Bunyeroo Formation: lonestones (★) with clasts of unreported roundness from one lithological group.
Insufficient	☆	0	Hongtiegou Formation: diamictite with subangular to subrounded clasts from one lithological group.

[a]Confidence weight relative to a five-star deposit (weight = 1) which is (almost) certain to be glaciogenic in origin. One- to five-star deposits follow a geometric relationship with a ratio of ½. Zero-star deposits are considered completely uninformative about the presence of ice during deposition on current evidence (weight = 0).
[b]No Ediacaran deposits identified in this study currently meet the five-star threshold (Tindal, 2023; Wong Hearing et al., 2026).

2.4 Palaeogeographic reconstructions

Uncertainty in reconstructing Ediacaran palaeogeography stems from uncertainty in how to interpret Ediacaran palaeomagnetic data (e.g. Domeier et al., 2023). The hypothesis of a true polar wander (TPW) event (e.g. Domeier et al., 2023; Wen et al., 2022) has recently been evaluated using candidate Ediacaran glaciogenic deposits and climate simulations (Liu et al., 2025; Wang et al., 2023a, b). Here we consider two other possible mid-Ediacaran palaeogeographic reconstructions that do not invoke a TPW event: PALEOMAP (Scotese, 2016; Scotese and Wright, 2018) and MERDITH2021 (Merdith et al., 2021). Although we consider the palaeolatitudinal positions of candidate glaciogenic deposits on both of these reconstructions, we focus on the PALEOMAP configuration for our model simulations because this is the only palaeogeography currently available with resolved topography and bathymetry (Scotese, 2016; Scotese and Wright, 2018). We use the 600 Ma configuration of both rotation models because the PALEOMAP rotation model has resolved topography and bathymetry for its 600 Ma time step, which is taken as representative of the mid-Ediacaran Gaskiers glaciation interval. The difference between the 600 Ma and 580 Ma configurations is negligible in comparison to the differences between rotation models.

We also draw comparisons between our results on the PALEOMAP and MERDITH2021 configurations and results from a study (Liu et al., 2025) using the TPW reconstruction. We note that the Wen et al. (2022) rotation model and its derivatives as

https://doi.org/10.5194/egusphere-2026-3617
Preprint. Discussion started: 30 June 2026

used in Liu et al. (2025) are not published, and our comparisons are therefore qualitative. Notable differences between the three configurations at 580 Ma, the earliest time step of the palaeogeography used in Liu et al. (2025), are as follows:

a. West Gondwana (North Africa and South America) is placed at mid- to high palaeolatitudes in the PALEOMAP and MERDITH2021 configurations, but low palaeolatitudes in the Wen et al. (2022) configuration,
b. Baltica (the Baltic region and Eastern Europe) is placed at mid- to high palaeolatitudes in the PALEOMAP and MERDITH2021 configurations, but low palaeolatitudes in the Wen et al. (2022) configuration, and
c. Laurentia (North America and Greenland) is placed at high southern latitudes in the PALEOMAP and Wen et al. (2022) configurations, but mid- to low latitudes in the MERDITH2021 configuration.

Temporally well-constrained geological evidence weighted by confidence in glaciogenicity should be able to discriminate between the substantial differences in the hypothesised positions of these three major palaeocontinents in the Ediacaran.

2.5 Climate and ice-sheet model simulations

We used general circulation model (GCM) and ice sheet model simulations to quantify the response of mid-Ediacaran climate and land ice to different atmospheric pCO_2 levels, following a similar but simpler approach to that of Pohl et al. (2016a) as outlined below.

2.5.1 General boundary conditions

All simulations used the 'mid-Ediacaran' (600 Ma) PALEOMAP palaeogeographic reconstruction (figs. S1-2; Scotese, 2016; Scotese and Wright, 2018) with the land surface defined as a rocky desert with an albedo of 0.24, modified by snow when present, due to the absence of land plants in the Ediacaran (e.g. Lenton et al., 2016). All simulations used a solar luminosity of 1303.12 Wm^{-2} (4.98 % weaker than present day) following Gough (1981). In the absence of reliable constraints on Ediacaran atmospheric composition, notably pCO_2 proxy data (e.g. Mills et al., 2025), we evaluated a range of pCO_2 values, from 1 to 32 times pre-industrial atmospheric levels (PAL = 280 ppmv). Note that we only vary atmospheric pCO_2 and not other atmospheric greenhouse gases, meaning that our simulations evaluate pCO_2-equivalent greenhouse gas forcing. In the absence of reliable constraints on Earth's orbital conditions beyond a few tens of millions of years (e.g. Laskar et al., 2004), we evaluated both a median orbital configuration similar to the present day (eccentricity: 0; obliquity: 23.5 °; date of perihelion: 21 March), and an orbital configuration that favours a warm austral summer (eccentricity: 0.07; obliquity: 23.5 °; date of perihelion: 29 December) which would tend to inhibit Southern Hemisphere ice sheet growth.

2.5.2 FOAM general circulation model simulations

We used the Fast Ocean Atmosphere Model (FOAM) version 1.5 (Jacob, 1997) general circulation model (GCM) to simulate mid-Ediacaran climate conditions. The quick turnaround time of FOAM makes it suitable for deep-time palaeoclimate studies where a wide range of loosely constrained boundary conditions need to be evaluated (e.g. Pohl et al., 2016a; Wong Hearing et al., 2021). FOAM is a mixed-resolution coupled ocean-atmosphere GCM with no flux corrections. The atmosphere module is

https://doi.org/10.5194/egusphere-2026-3617
Preprint. Discussion started: 30 June 2026

a parallelised version of the National Center for Atmospheric Research (NCAR) Community Climate Model 2 (CCM2) with upgraded radiative and hydrologic physics from CCM3 version 3.2. The atmosphere module is run with R15 spectral resolution (4.5° × 7.5°) and 18 vertical levels. The ocean module is Ocean Model version 3 (OM3), which is run with 2.8° × 1.4° longitude–latitude resolution and 24 vertical levels. Sea ice is simulated by the NCAR Climate System Model 1.4 sea ice module. The FOAM simulations were initialised with a warm ice-free ocean of homogeneous salinity of 35 ‰. FOAM simulations were run for 2000 years to allow the deep ocean to approach equilibrium. Each run was extended by 50 years with the monthly output saved to produce the climatology files. The FOAM climatology files are available in Data S3. The FOAM simulations were used both to compare simulated sea-ice extent with geological data and to provide sea-surface temperature fields used as boundary conditions for the higher-resolution LMDZ atmosphere-only simulations.

2.5.3 LMDZ atmospheric circulation simulations

The LMDzOR model consists of the atmospheric general circulation model LMDz6 (Hourdin et al., 2020) coupled with the land surface ORCHIDEE model (Krinner et al., 2005). The atmospheric grid has a resolution of 2.5° in longitude and 1.26° in latitude (144 x 142 longitude-latitude grid), with 79 vertical layers extending from the surface to an altitude of 80 km. The LMDz dynamical core is based on finite difference and finite volume discretization of the primitive equations governing atmospheric dynamics and physics, coupled to a suite of physical parameterizations (Hourdin et al., 2020). The radiative transfer is handled by the Rapid Radiative Transfer Model (Mlawer et al., 1997). The land surface ORCHIDEE includes a river runoff module that routes the water on the continents (d'Orgeval et al., 2008). Vegetation is simulated through 11 plant functional types, among which one PFT corresponds to bare soil, which was prescribed here.

The prescribed boundary conditions for the Ediacaran include palaeogeography, bare soil terrestrial surface, monthly mean sea surface temperature, and sea ice fraction derived from FOAM simulations and interpolated onto the higher-resolution LMDz6 grid. No continental ice sheets were included. The solar constant and orbital parameters were set to produce the same daily incoming solar flux as in the FOAM simulations. Due to numerical instabilities, the LMDz6 model was unable to reach equilibrium at a pCO_2 of 32 PAL. Simulations were run for 50 years, and outputs were averaged over the last 10 years. The LMDzOR outputs provided monthly mean surface air temperature and precipitation fields used as input for the ice-sheet model simulations.

2.5.4 GRISLI ice sheet simulations

We used the GRenoble Ice-Shelf and Land Ice (GRISLI) model to simulate Southern Hemisphere glacial onset. GRISLI is a three-dimensional ice-sheet model that accounts for both temperature and ice velocity, simulating both grounded and floating ice as ice sheets, ice streams, and ice shelves using a 40 km x 40 km resolution grid (Ritz et al., 2001). The type of ice (or none) in each grid cell is determined for each time step. The initial (monthly) surface air temperature and precipitation fields were provided by the LMDZ atmosphere simulations. These fields were subsequently updated throughout ice-sheet model integration time as a function of ice-sheet height, using an adiabatic lapse rate (5 K km^{-1}) for surface air temperature and an

https://doi.org/10.5194/egusphere-2026-3617
Preprint. Discussion started: 30 June 2026

exponential law for precipitation (based on the Clausius-Clapeyron dependency). These online corrections permit capture of the impact of land ice on local climate. They do not, however, permit account of the feedbacks of the ice sheet on climate (including ocean and atmospheric dynamics) as would do a coupled climate-ice-sheet model. The resolution of the FOAM ocean module is insufficient to simulate melting underneath ice shelves, so we imposed a melting rate of 0.2 m a^{-1} on continental shelves (depth ≤600 m) and 2 m a^{-1} beyond continental shelves (depth >600 m) (Pohl et al., 2016a). In our simulations, the vast majority of ice remained grounded. GRISLI simulates ice-sheet evolution in response to climate with a surface mass balance equating to the sum of accumulation minus ablation following mean monthly surface temperature and precipitation. Ablation follows the positive degree day method with a surface melt refreezing rate of 60 % and air temperature variability (standard deviation) of 5 K over each month. Isostatic adjustment of the bedrock due to ice loading is accounted for using the parameterised elastic lithosphere/relaxing asthenosphere (ELRA) model with a standard relaxation time of 3 kyr.

3. Results

3.1 Geological evidence for mid-Ediacaran glaciation

We evaluated 91 candidate glaciogenic deposits for which a mid-Ediacaran age has been suggested (Fig. 1; Supplementary Information; Data S1). All of the deposits considered here have some relevant dating evidence, even if the age constraints are sometimes poor. These deposits fall into two groups of distinct depositional ages (Wong Hearing et al., 2026): (1) those older than ~579 Ma, and (2) those younger than ~565 Ma (Fig. 1). A systematic evaluation of the available geochronological and stratigraphic constraints revealed that many deposits in the older group are substantially older and, in fact, probably Cryogenian in age (Wong Hearing et al., 2026). Here, we focus on those deposits with plausible depositional ages between 635 to 579 Ma, i.e. early to mid-Ediacaran, of which there are 28, of which 22 are identified as most likely being deposited in the MEIH, between ~593 to 579 Ma (

; Data S1; Data S6).

Of these 22 candidate MEIH deposits, five obtained a three-star score and 10 obtained a four-star score (

). No Ediacaran deposits have so far received a five-star rating (Tindal, 2023; Wong Hearing et al., 2026). Several three- and four-star mid-Ediacaran deposits are located on the Avalonia, Baltica, and West Gondwana (North Africa and South America) palaeocontinents. There are no three- and four-star deposits from the Laurentia, Siberia, or South China palaeocontinents during the MEIH (Fig. 2). Most candidate glaciogenic deposits on the North China Craton and surrounding terranes (e.g. Qaidam, Tarim) likely fall into the post-565 Ma suite of deposits (e.g. Wang et al., 2021; Wong Hearing et al., 2026; Xiao et al., 2004) and are not considered further here. The Fengtai Formation from the North China Craton (Tan et al., 2025; Yue et al., 2025) is plausibly of MEIH age but is given a two-star score here (see Supplementary Information). The four-star Xichangjing Formation is plausibly of MEIH age and was deposited on the northern margin of either the North China or Tarim cratons (regional correlation is uncertain; Niu et al., 2024). The only three-star deposit from East Gondwana is the Croles Hill diamictite (Tasmania, Australia) which is well dated to the late MEIH interval (Calver et al., 2026); it is parsimoniously interpreted as a submarine mass flow deposit in a tectonically active setting with or without a glaciogenic interpretation (Supplementary Information; Mulder et al., 2020).

https://doi.org/10.5194/egusphere-2026-3617
Preprint. Discussion started: 30 June 2026

There is evidence for multiple local advances and retreats of ice sheets during the MEIH on Avalonia, Baltica, and West Gondwana (Supplementary Information). In particular, repeated ice-sheet fluctuations are supported by likely glaciogenic diamictites alternating with shales and sandstones throughout the Tiddiline Group (North African Gondwana) (Letsch et al., 2018) and Glussk Formation (Baltica) (Chumakov, 2004), as well as in parasequences developed in the Rocky Harbour Formation in and between the Trinity and Mercantile diamictites (Avalonia) (Gómez et al., 2026).

3.2 Palaeolatitudinal extent of geological evidence

The reconstructed palaeolatitudinal extent of the candidate mid-Ediacaran glaciogenic deposits depends on the chosen rotation model (

; Data S6). The PALEOMAP (Scotese, 2016; Scotese and Wright, 2018) and MERDITH2021 (Merdith et al., 2021) rotation models produce quantitatively but not qualitatively different results (Fig. 2; Fig. 3;

), with the majority of high-scoring mid-Ediacaran deposits positioned polewards of 30° latitude in both reconstructions. Following the three-star threshold for plausible glaciogenicity detailed above, it is only on the PALEOMAP rotation model that the Croles Hill diamictite and Xichangjing Formation are reconstructed at lower latitudes (7.2 °N and 14.5 °N, respectively). On the MERDITH2021 rotation model, the Crole Hill diamictite is reconstructed at 1.1 °S latitude, and the four-star Las Ventanas and correlative three-star Playa Hermosa formations (Rio de la Plata craton) are reconstructed at lower latitudes (26.9 °S and 26.2 °S, respectively). As noted above, the Croles Hill diamictite is parsimoniously interpreted as a submarine mass flow deposit (Supplementary Information). All other low palaeolatitude outliers are rated less than three stars or are of uncertain Ediacaran age.

On the PALEOMAP rotation model, three-star deposits have a median absolute palaeolatitude of 28.2° (mean = 33.6°; standard deviation [s.d.] = 24.9°) and four-star deposits have a median absolute palaeolatitude of 57.3° (mean = 51.1°; s.d. = 24.6°) (

). On the MERDITH2021 rotation model, three-star deposits have a median absolute palaeolatitude of 39.7° (mean = 33.9°; s.d. = 21.0°) and four-star deposits have a median absolute palaeolatitude of 43.3° (mean = 41.9°; s.d. = 8.5°) (

).

https://doi.org/10.5194/egusphere-2026-3617
Preprint. Discussion started: 30 June 2026

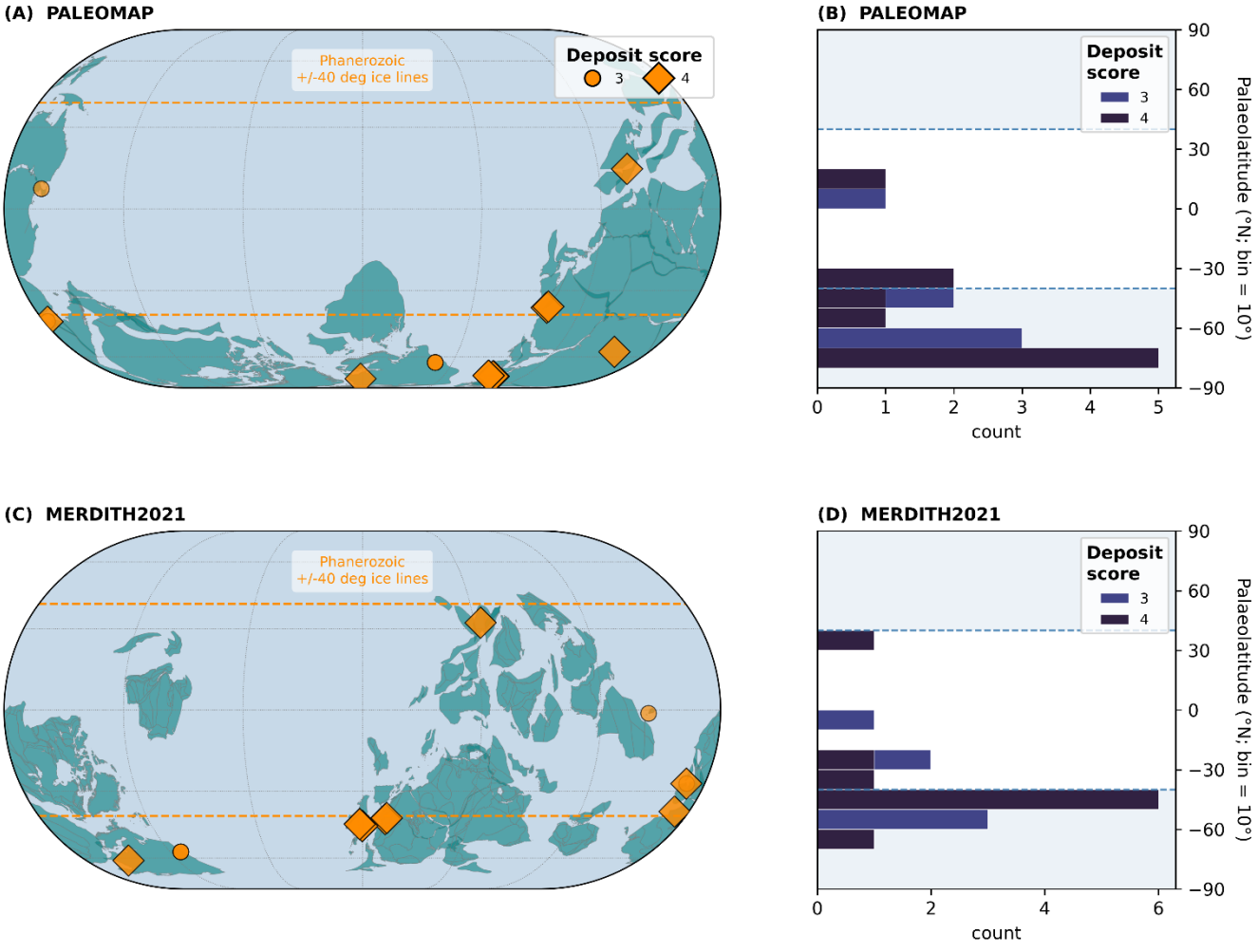

Fig. 2. Palaeogeographic and palaeolatitudinal distribution of candidate mid-Ediacaran glaciogenic deposits rated at least three stars on two rotation models at 600 Ma. (A, B) PALEOMAP rotation model (Scotese, 2016; Scotese and Wright, 2018). (C, D) MERDITH2021 rotation model (Merdith et al., 2021). All panels show likely MEIH deposits rotated to 600 Ma to match the rotation of the mid-Ediacaran PALEOMAP palaeogeographic reconstruction (Scotese, 2016; Scotese and Wright, 2018) used in the climate model simulations below. Dashed lines at ±40° latitude show the typical Phanerozoic ice line (Table 1). See Data S1 and Data S6.

https://doi.org/10.5194/egusphere-2026-3617
Preprint. Discussion started: 30 June 2026

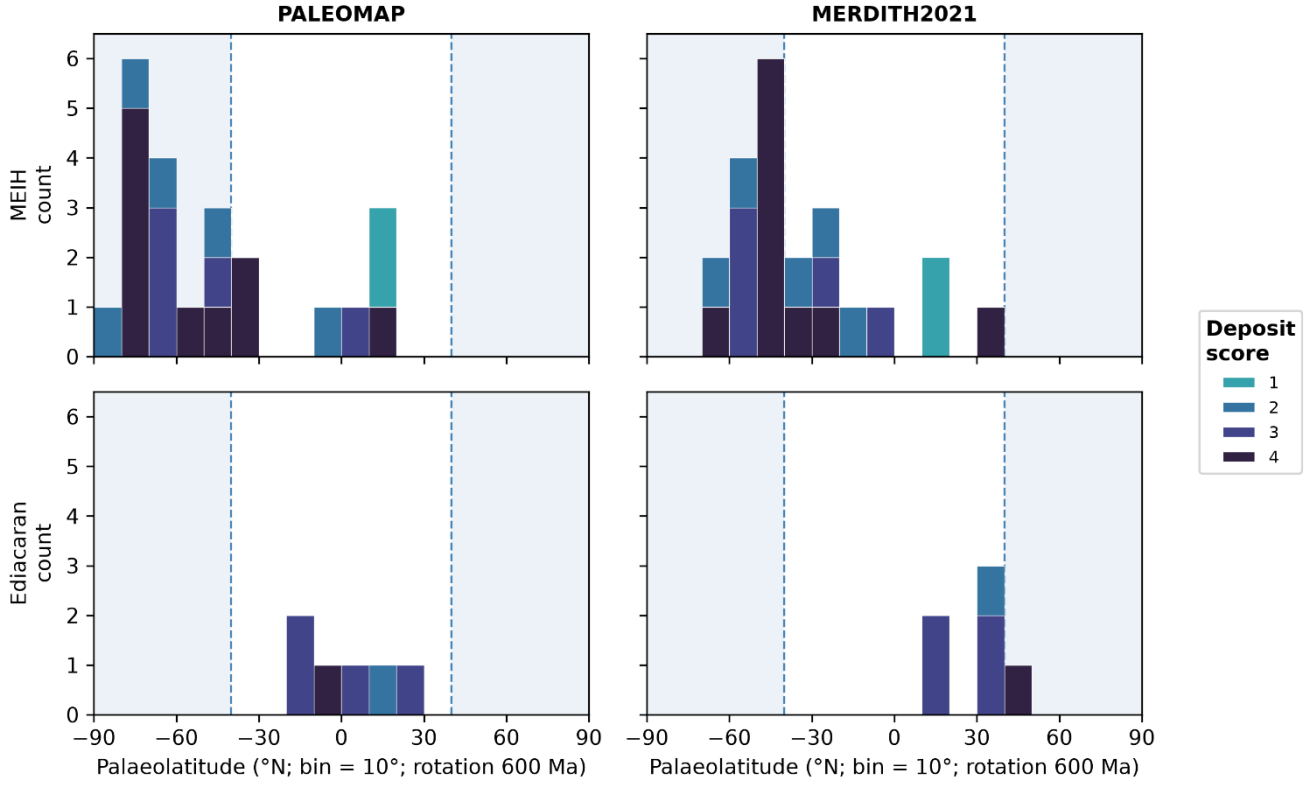

Fig. 3. Palaeolatitudinal extent of candidate mid-Ediacaran glaciogenic deposits on the PALEOMAP (Scotese, 2016; Scotese and Wright, 2018) and MERDITH2021 (Merdith et al., 2021) rotation models by likely age interval and star rating. The dashed blue lines and shaded blue regions show the typical ±40° latitude Phanerozoic ice line (Table 1). MEIH: deposits constrained to the mid-Ediacaran icehouse (~593 to 579 Ma); Ediacaran: deposits that are only constrained to an Ediacaran age (younger than Cryogenian, older than Cambrian). All deposits were palaeo-rotated to 600 Ma to match the mid-Ediacaran PALEOMAP palaeogeography used in the climate simulations. The patterns are similar for both models with rotation ages between 600 to 580 Ma. See Data S1 and Data S6.

https://doi.org/10.5194/egusphere-2026-3617
Preprint. Discussion started: 30 June 2026

Table 4. Summary statistics of the candidate mid-Ediacaran glaciogenic deposits. See Data S1 for full dataset and the Supplementary Code and Data S6 for the deposit rotations. All data points rotated to 600 Ma; MEIH: mid-Ediacaran icehouse; min.: minimum; s.d.: standard deviation.

	Number of deposits[a]			PALEOMAP absolute latitude				MERDITH2021 absolute latitude			
Score	**all**	**MEIH**	**Ediacaran**	**Min.**	**median**	**mean**	**s.d.**	**Min.**	**median**	**mean**	**s.d.**
all	28	22	6	5.1	42.9	42.7	26.7	1.1	39.7	36.2	16.6
4	11	10	1	8.7	57.3	51.1	24.6	27	43.3	41.9	8.5
3	9	5	4	6	28.2	33.6	24.9	1.1	39.7	33.9	21
2	6	5	1	5.1	55.8	49.4	32.3	12.8	31.7	36.7	18.6
1	2	2	0	16.7	18	18	1.9	12	13.5	13.5	2

[a]Number of deposits subdivided as follows: "all" = all of MEIH and Ediacaran; "MEIH" = deposits confidently assigned to the MEIH age range (~593 to 579 Ma); "Ediacaran" = deposits that can only be constrained to an Ediacaran age range (635 to 538.8 Ma).

https://doi.org/10.5194/egusphere-2026-3617
Preprint. Discussion started: 30 June 2026

3.3 Palaeoclimate simulations

Our FOAM GCM simulations indicate that sea ice can form at high southern latitudes even under quite high greenhouse gas levels (up to at least 32 PAL pCO_2-equivalent in FOAM; figs. S3-4). In contrast, in the Northern Hemisphere, where high latitude continents are absent, sea ice forms only under lower pCO_2 forcings (≤7 PAL pCO_2-equivalent in FOAM; figs. S3-4). Our simulations indicate that a sudden global climate cooling accompanied by an expansion of sea ice into the middle latitudes occurs if atmospheric pCO_2 decreases from 6 PAL to 4 PAL (figs. S3-4). A similar climatic instability has previously been reported for Late Ordovician FOAM simulations and attributed to the effects of an oceanic (northern) hemisphere on the ocean heat transport (Pohl et al., 2014, 2016b), a mechanism that may also apply to the MEIH interval.

3.4 Ice sheet growth

To simulate the conditions for mid-Ediacaran Southern Hemisphere ice sheet growth, we employed the higher resolution atmosphere GCM LMDz6, forced with FOAM-derived sea-surface temperature fields (see Methods). The resulting atmospheric outputs were then used to force the three-dimensional GRenoble Ice-Shelf and Land-Ice (GRISLI) ice sheet model which ran for 300 kyrs. A similar coupling strategy, but with a different orbital configuration, has been employed to investigate glacial onset in the Cretaceous (Ladant and Donnadieu, 2016), ice sheet evolution across the Eocene-Oligocene transition (Ladant et al., 2014), and Late Ordovician glaciation (Pohl et al., 2016a).

Results from our GRISLI model simulations indicate that, with the mid-Ediacaran (600 Ma) PALEOMAP palaeogeography, a moderate-sized ice sheet would have been initiated with a pCO_2-equivalent greenhouse gas level of 16 PAL, and possibly higher, even under unfavourable orbital configurations (Fig. 4). At 16 PAL and 12 PAL, the simulated ice sheet consists primarily of a single dome restricted to latitudes greater than 65 °S (Fig. 4c,d). However, when pCO_2 is reduced to 8 PAL and then 6 PAL, the main ice sheet extends slightly equatorward and a secondary nucleation centre develops near 40 °S, facilitated by topographic highs (Fig. 4a,b). There is generally good agreement between the centres of ice sheet initiation in our simulations and the palaeo-positions of three-star and four-star deposits in the Ediacaran rock record (Fig. 4). Note that we have not simulated the maximum extent of ice sheets or their minimum formation conditions, only the regions in which they start to form. Deposits located away from our simulated ice sheets are close to reconstructed topographic highs (Scotese and Wright, 2018) and may represent a more fully developed ice sheet or relate to mountain glacier ice (*sensu* Niu et al., 2024).

https://doi.org/10.5194/egusphere-2026-3617
Preprint. Discussion started: 30 June 2026

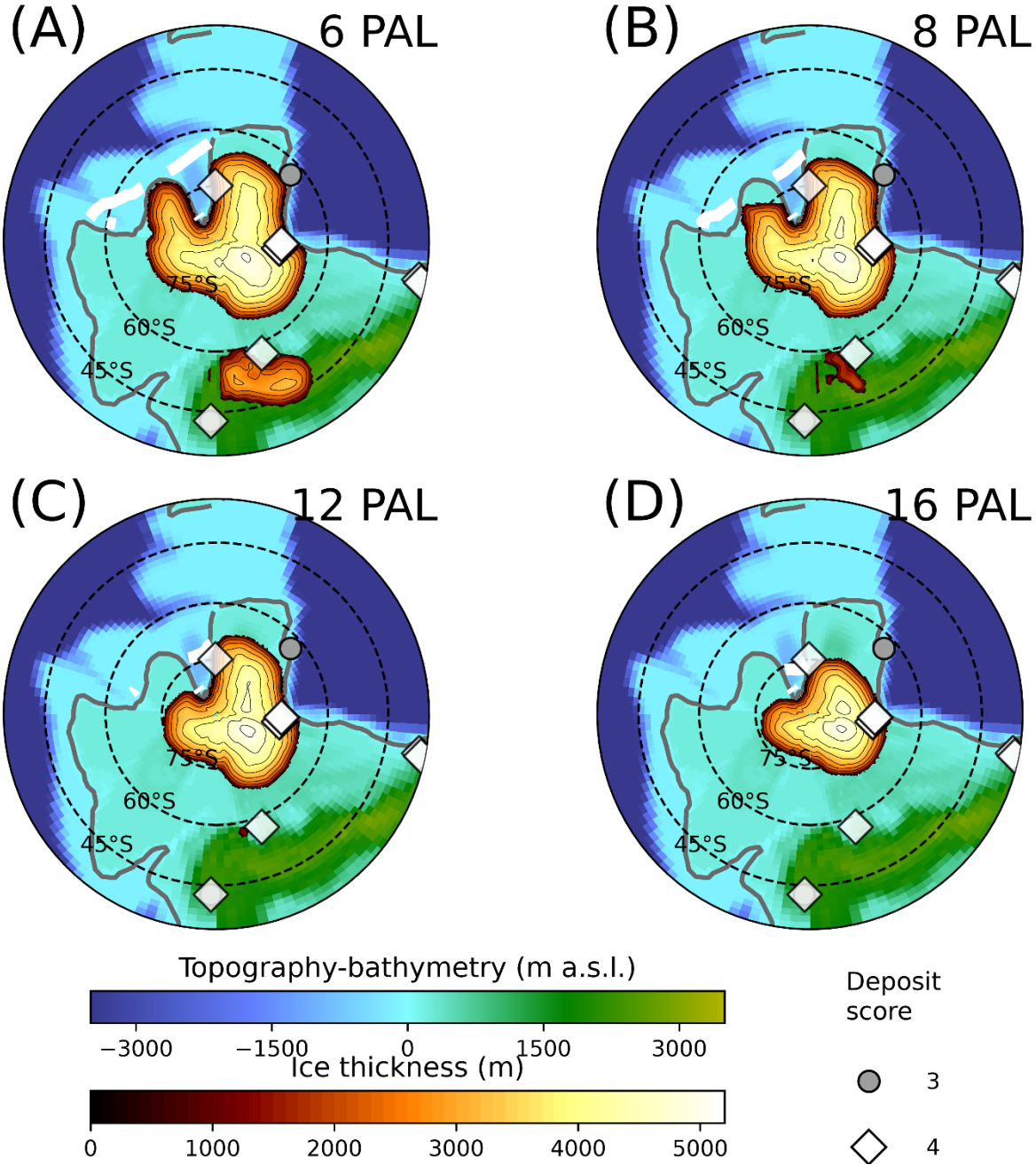

370 **Fig. 4. Ice sheet model simulations for MEIH glacial onset for (A) 6, (B) 8, (C) 12, and (D) 16 times pre-industrial atmospheric level (PAL) pCO_2 (1 PAL = 280 ppmv). Each panel shows the GRISLI-simulated ice sheet thickness (heatmap colours), the extent of the FOAM-simulated mean annual 50 % sea ice fraction (thick white lines), and MEIH deposits rated at least three stars (diamonds) overlain on the topography and bathymetry ("m a.s.l.": metres above sea level) used as boundary conditions for the simulations. There is remarkably good correspondence between the palaeo-rotated positions of candidate glaciogenic deposits and the initial ice**
375 **sheet developing around the South Pole and southern highlands. Ice sheet thickness simulated at equilibrium after 300 kyr of ice**

https://doi.org/10.5194/egusphere-2026-3617
Preprint. Discussion started: 30 June 2026

sheet model integration. The topography includes no highlands at the South Pole (see figs. S1-2). The map is a south polar projection with latitudes shown every 15 ° between 90 to 45 °S and map margin at 35 °S. See Data S5 and Data S6.

4 Discussion

4.1 Timing and geography of the mid-Ediacaran icehouse

Taking together the geological evidence and climate simulations, our results support a 10 to 15 Myr icehouse interval that terminated at 579 Ma (Fig. 1; Wong Hearing et al., 2026) characterised by grounded ice at high to mid-latitudes (Fig. 2; Fig. 3; Fig. 4;). This was followed by a gap in the record of glaciogenic deposits lasting at least 14 Myr, which likely reflects a greenhouse climate state including over the Shuram carbon isotope excursion interval (~574 to 567 Ma; e.g. Shields et al., 2019; Wong Hearing et al., 2026). The number and tempo of possible glacial-interglacial cycles (e.g. the parasequences reported by Gómez et al., 2026) in the MEIH interval remain unresolved, but further field work may help clarify this as astronomically-forced cyclicity has been interpreted in rocks deposited during the subsequent Shuram negative CIE (e.g. Minguez et al., 2015), suggesting that it is possible in rocks of this age.

Our analysis supports a high to mid-latitude distribution of ice sheets during the MEIH, even accounting for some uncertainty in Ediacaran palaeogeography (Fig. 2; Fig. 3). The MERDITH2021 rotation model implies grounded ice at slightly lower palaeolatitudes than the PALEOMAP rotation model, but both are consistent with the observed latitudinal distributions of Phanerozoic glaciogenic deposits (e.g. Evans, 2003; Macdonald et al., 2019; Merdith et al., 2025). However, under the debated (Domeier et al., 2023) hypothesis of one or more Ediacaran true polar wander events, those continental reconstructions (e.g. Wen et al., 2022) place Laurentia at very high palaeolatitudes around 580 Ma whilst placing Baltica and North Africa at very low palaeolatitudes. Laurentia lacks robust evidence for glaciation at this time, whereas glacial deposits are well developed in both Baltica and North Africa. We suggest, therefore, that both the PALEOMAP (Scotese, 2016; Scotese and Wright, 2018) and Wen et al. (2022) configurations do not adequately resolve the position of Laurentia during this interval, having it at too high a latitude. Similarly, the equatorial positions of North African West Gondwana and Baltica in the Wen et al. (2022) configuration at 580 Ma are not supported by the geological data. Rather, the high to mid-palaeolatitude positions of West Gondwana and Baltica as reconstructed in both the PALEOMAP (Scotese, 2016; Scotese and Wright, 2018) and MERDITH2021 (Merdith et al., 2021) configurations are in better agreement with the geological data and our model simulations. The position of the North China and adjacent cratons, including Tarim, are also uncertain in the Ediacaran. Our data support a higher latitude position than is currently resolved in the PALEOMAP configuration (Fig. 2). We suggest that the distribution of robustly identified and temporally-constrained glaciogenic deposits can serve as a test dataset for hypotheses of Ediacaran palaeogeography and may help to resolve some of the enduring palaeogeographic enigmas of this interval.

4.2 Model support for a Laurentide-like MEIH ice sheet

Our model simulations support a Phanerozoic-style icehouse as a plausible scenario for mid-Ediacaran climate state. The pCO_2 threshold for the initiation of mid-Ediacaran land ice growth (>16 PAL) is higher than that estimated for the Late Ordovician

https://doi.org/10.5194/egusphere-2026-3617
Preprint. Discussion started: 30 June 2026

(12 PAL) , likely due to a weaker solar luminosity. Our simulations do not account for the cooling effect of land ice on regional climate through albedo-temperature feedbacks and therefore substantially underestimate the extent that the ice sheet would reach under climate-ice sheet equilibrium. Pohl et al. (2016a), employing a similar modelling strategy with a comparable continental configuration for the Late Ordovician (~450 Ma), demonstrated that accounting for the feedbacks of land ice growth on global climate systematically led to a further expansion of simulated ice sheets to 40 °S, consistent with Phanerozoic and now Ediacaran geological evidence (Fig. 5). These large ice sheets developed at pCO_2 levels above the pCO_2 threshold for sudden sea ice advance and climate cooling, which is found between 6 PAL and 4 PAL in our mid-Ediacaran simulations. On crossing the climate instability threshold, the Late Ordovician ice sheet further extended to 30 °S (Pohl et al., 2016a). This previous modelling work for the Late Ordovician suggests that the ice sheets simulated for pCO_2 levels as high as 16 PAL in the mid-Ediacaran (Fig. 4) would similarly reach ~40 °S when the land ice-climate feedbacks are accounted for, and that a pCO_2 drop below 6 PAL may trigger an additional ice sheet advance to ~30 °S. The presence of large glacial centres at the middle latitudes in simulations at 8 PAL and 6 PAL (Fig. 4a,b), even without accounting for ice sheet-climate feedbacks, lends strong support to the capacity of our simulated ice sheets to reach the middle latitudes, likely supported by the concentration of continents at high southern latitudes. This implies that a broad range of pCO_2 values, at least as high as 16 PAL (corresponding to a global mean surface air temperature of 21.2 °C before accounting for ice sheet feedbacks), would be compatible with a mid-Ediacaran ice sheet expanding to between ~40 to 30 °S, comparable with Phanerozoic icehouse intervals.

As briefly discussed above, a recent study examined the use of snow cover as a proxy for land ice extent in the late Ediacaran and concluded that a narrow range of low pCO_2 values, between 35 to 280 ppmv (0.125 to 1 PAL), corresponding to very cold global mean surface temperatures between –4.2 to +1.6 °C, were required to sustain Ediacaran ice sheets (Liu et al., 2025). Direct comparison with the results of Liu et al. (2025) is complicated by major differences in modelling strategies, notwithstanding the questions of palaeogeography discussed above. However, several factors may have rendered glacial conditions more difficult to achieve in their set-up, including a coarser horizontal resolution of the atmospheric model (3.75° × 3.75°, compared to 2.5° × 1.3° in our study) and the absence of highlands serving as land ice nucleation centres (e.g. Ladant and Donnadieu, 2016; Pohl et al., 2016a).

The geometry of our simulated ice sheets, comprising a main dome and decreasing ice thickness towards the margins, resembles the geometry of the Antarctic ice sheet (e.g. Quiquet et al., 2018), and the reconstructed geometries of the Laurentide ice sheet during the last glaciation (e.g. Quiquet et al., 2021) and other Phanerozoic ice sheets (e.g. Pohl et al., 2016a). The reversed gradient in land ice thickness simulated in Liu et al. (2025) may partly arise from the imposed monotonically decreasing topography from the continental interior to the coast, and from the shorter integration time of the ice sheet model (100 kyr compared with 300 kyr in our study). In particular, we note that the early stages of ice sheet development in our simulations resemble those of Liu et al. (2025) (i.e. with maximum land ice thickness in coastal areas where precipitation is highest; contrast Fig. 4 with Fig. S5).

https://doi.org/10.5194/egusphere-2026-3617
Preprint. Discussion started: 30 June 2026

Future studies employing coupled climate-ice sheet models fully accounting for the feedbacks of land ice on climate will be essential to refining our understanding of mid-Ediacaran glacial onset and ultimate ice sheet geometry, as well as their sensitivity to model parameters and boundary conditions including hypothesised palaeogeographies. Coupled climate-ice sheet models in deep time require very long model integration times (>300 kyrs) and asynchronous coupling methods are difficult to employ at scale, meaning that few studies have attempted to apply such work in deep time contexts (Herrington and Poulsen, 2011; Pohl et al., 2016a). Recent developments in Earth system models of intermediate complexity offer promising avenues for advancing this field (Leloup et al., 2025; Willeit et al., 2022), although these models have the caveat of reduced robustness of the atmospheric component.

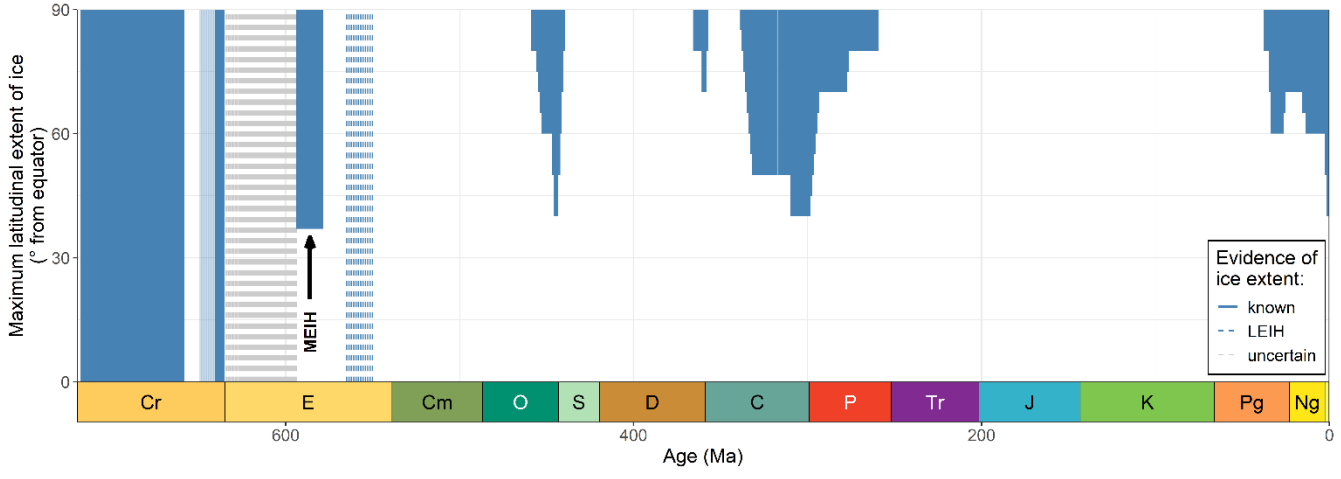

Fig. 5. Latitudinal extent of land ice from the Cryogenian to the present day derived from glaciogenic sedimentary deposits. Blue bars indicate the known latitudinal extent of ice at different times; the light blue bar indicates uncertainty in the timing of Marinoan glaciation onset (Hoffman et al., 2017); the dashed blue bar indicates the duration of the late Ediacaran icehouse (LEIH) which had an uncertain but not global palaeolatitudinal extent (Wong Hearing et al., 2026); the dashed grey bar indicates uncertainty about what if any land ice (e.g. Lan et al., 2024) was present in the early Ediacaran, for which there is little data; arrow and "MEIH" point to the mid-Ediacaran icehouse. See Error! Reference source not found.**.**

4.3 Potential controls on mid-Ediacaran climate state

Phanerozoic icehouse climate states have likely been triggered and sustained by a complex interplay of multiple Earth system mechanisms whose relative significance varies over time (e.g. Merdith et al., 2025). Macdonald et al. (2019) argued that Phanerozoic icehouse intervals are closely correlated with enhanced tectonic activity within ±20 ° latitude of the equator, and in particular that longer arc-continent sutures in the tropics lead to greater exposure of mafic igneous rocks hence to higher weathering rates in the tropics. This mechanism thereby enhances CO_2 drawdown via silicate weathering, driving global climate toward colder conditions (Macdonald et al., 2019). This hypothesis has not been formally evaluated for the Ediacaran, but some plate reconstructions suggest that the mid- to late Ediacaran assembly of Gondwana and accretion of various terranes

https://doi.org/10.5194/egusphere-2026-3617
Preprint. Discussion started: 30 June 2026

around East Gondwana (Antarctica and Australia) (e.g. Cawood et al., 2021) may conceivably have contributed to increased weatherability in the tropics. However, it is unlikely that a single driver was responsible for the MEIH, as the prolonged icehouse climates of the Phanerozoic could only be initiated and sustained through the interaction of several solid-Earth cooling mechanisms (Merdith et al., 2025).

Solid-Earth processes may also have played a role in terminating the MEIH. It has been suggested that volcanic degassing from two large igneous provinces (LIPs), the Central Iapetus Magmatic Province (CIMP) and the Volyn LIP, raised atmospheric greenhouse gas levels, thereby ending icehouse conditions in the mid-Ediacaran (Środoń et al., 2023; Youbi et al., 2020) and perhaps contributed to the Shuram carbon isotope excursion, which marks a major perturbation to the global carbon cycle (Youbi et al., 2020). It has further been suggested that oxidation of a reservoir of dissolved organic carbon (DOC) may have driven elevated atmospheric pCO_2 and sustained high temperatures throughout the Shuram excursion interval (Shields et al., 2019). As with the onset of the MEIH, there were likely a suite of driving mechanisms to its termination, with their relative weights yet to be determined.

5 Conclusions

Here, we have outlined the essential dimensions of Earth's climate state in the middle Ediacaran. Following non-TPW hypotheses for Ediacaran palaeogeography implies that the spatial distribution of geological evidence for the MEIH was similar to that of Phanerozoic icehouse intervals, with glacial deposits concentrated in high to mid-latitudes. In contrast, plate rotation models designed to accommodate TPW events produce palaeogeographic reconstructions that are climatically at odds with the spatio-temporal distribution of robustly identified mid-Ediacaran glaciogenic deposits. Here we wish to underscore that climatically sensitive lithologies can be invaluable resources for evaluating hypotheses of palaeogeography and further emphasise the need to be sure about the depositional interpretations of all lithology occurrences used for ground-truthing palaeogeographic hypotheses.

Our results indicate a relatively abrupt shift from icehouse to greenhouse conditions at ~579 Ma recorded on several palaeocontinents, before the earliest records of complex macroscopic marine animal life (e.g. Boag et al., 2024; Matthews et al., 2021; Pu et al., 2016). The apparently abrupt termination of the MEIH may support the use of glaciostratigraphy in subdividing the Ediacaran System (Xiao and Narbonne, 2020). Our analysis identifies the need to further resolve the precise correlation of specific glacial deposits, and especially the timing and extent of the subsequent late Ediacaran icehouse interval (Wong Hearing et al., 2026). The onset and termination conditions of the MEIH, including palaeogeography, atmospheric composition, and internal dynamics of this icehouse interval, should be considered priority targets for future research.

https://doi.org/10.5194/egusphere-2026-3617
Preprint. Discussion started: 30 June 2026

Code availability

The code used to generate the analyses and figures for this manuscript are available at https://github.com/twwh01/MEIH. The model code for GRISLI is available at https://forge.ipsl.jussieu.fr/grisli.

Data availability

All data underlying our manuscript are available either in the main text, supplement, or archived on Zenodo at https://doi.org/10.5281/zenodo.17158910.

Supplement link

the link to the supplement will be included by Copernicus, if applicable

Author contribution

Conceptualization: TWWH, MW, AP, THPH. Methodology: TWWH, AP, MW, FF, BHT. Investigation: TWWH, AP, FF, TMV, BHT. Visualization: TWWH, AP. Writing—original draft: TWWH, MW. Writing—review & editing: AP, THPH, AGL, BHT, TMV, FF, TWWH, MW.

Competing interests

The authors declare that they have no conflict of interest.

Acknowledgements

We are grateful to Graham Shields for helpful discussions on specific deposits, and Neil Davies for discussions on methodology and database development. Claude Code was used to perform code reviews and refactoring.

Financial support

The Leverhulme Trust research grant RPG-2022-233 to MW, THPH, AGL, and AP. AP acknowledges the support of the French *Agence Nationale de la Recherche* (ANR) under reference ANR-22-CE01-0003 (project ECO-BOOST). Calculations were performed using HPC resources from DNUM CCUB (*Centre de Calcul de l'Université de Bourgogne*). BHT acknowledges support from NERC C-CLEAR DTP studentship NE/R009457/1.

https://doi.org/10.5194/egusphere-2026-3617
Preprint. Discussion started: 30 June 2026

Review statement

the review statement will be included by Copernicus

References

Bendtsen, J.: Climate sensitivity to changes in solar insolation in a simple coupled climate model, Climate Dynamics, 18, 595–609, https://doi.org/10.1007/s00382-001-0198-4, 2002.

Boag, T. H., Busch, J. F., Gooley, J. T., Strauss, J. V., and Sperling, E. A.: Deep-water first occurrences of Ediacara biota prior to the Shuram carbon isotope excursion in the Wernecke Mountains, Yukon, Canada, Geobiology, 22, e12597, https://doi.org/10.1111/gbi.12597, 2024.

Bowyer, F. T. and Nelson, L. L.: Reviewing chronostratigraphic uncertainty of the Ediacaran–Cambrian transition, Journal of the Geological Society, in press, jgs2025-100, https://doi.org/10.1144/jgs2025-100, 2026.

Budyko, M. I.: The effect of solar radiation variations on the climate of the Earth, Tellus, 21, https://doi.org/10.3402/tellusa.v21i5.10109, 1969.

Busch, J. F., Boag, T. H., Sperling, E. A., Rooney, A. D., Feng, X., Moynihan, D. P., and Strauss, J. V.: Integrated Litho-, Chemo- and Sequence Stratigraphy of the Ediacaran Gametrail Formation Across a Shelf-Slope Transect in the Wernecke Mountains, Yukon, Canada, American Journal of Science, 323, 4, https://doi.org/10.2475/001c.74874, 2023.

Calver, C. R., Cumming, G. V., Halverson, G. P., Crowley, J. L., Roberts, N. J., and Schmitz, M.: High-resolution U-Pb dating of the Croles Hill Diamictite, Tasmania: Near-synchroneity of widely separated mid-Ediacaran glacial deposits, Precambrian Research, 432, 107958, https://doi.org/10.1016/j.precamres.2025.107958, 2026.

Carto, S. L. and Eyles, N.: Chapter 43 The Squantum Member of the Boston Basin, Massachusetts, USA, Geological Society, London, Memoirs, 36, 475–480, https://doi.org/10.1144/M36.43, 2011.

Cawood, P. A., Martin, E. L., Murphy, J. B., and Pisarevsky, S. A.: Gondwana's interlinked peripheral orogens, Earth and Planetary Science Letters, 568, 117057, https://doi.org/10.1016/j.epsl.2021.117057, 2021.

Chumakov, N. M.: Trends in global climatic changes inferred from geological date, Stratigraphy and Geological Correlation, 12, 117–138, 2004.

Chumakov, N. M.: The Baykonurian glaciohorizon of the Late Vendian, Stratigr. Geol. Correl., 17, 373–381, https://doi.org/10.1134/S0869593809040029, 2009.

Cohen, K., Harper, D., Gibbard, P., and Car, N.: The ICS international chronostratigraphic chart this decade, Episodes Journal of International Geoscience, 48, 105–115, https://doi.org/10.18814/epiiugs/2025/025001, 2025.

Domeier, M., Robert, B., Meert, J. G., Kulakov, E. V., McCausland, P. J. A., Trindade, R. I. F., and Torsvik, T. H.: The enduring Ediacaran paleomagnetic enigma, Earth-Science Reviews, 242, 104444, https://doi.org/10.1016/j.earscirev.2023.104444, 2023.

Evans, David. A. D.: A fundamental Precambrian–Phanerozoic shift in earth's glacial style?, Tectonophysics, 375, 353–385, https://doi.org/10.1016/S0040-1951(03)00345-7, 2003.

https://doi.org/10.5194/egusphere-2026-3617
Preprint. Discussion started: 30 June 2026

Evans, David. A. D. and Raub, T. D.: Chapter 7. Neoproterozoic glacial palaeolatitudes: a global update, in: The Geological Record of Neoproterozoic Glaciations, edited by: Arnaud, E., Halverson, G. P., and Shields-Zhou, G. A., Geological Society of London, London, UK, 93–112, 2011.

Fischer, A. G.: Climatic oscillations in the biosphere, in: Biotic Crises in Ecological and Evolutionary Time, edited by: Nitecki, M. H., Academic Press, 103–131, https://doi.org/10.1016/B978-0-12-519640-6.50012-0, 1981.

Fitzgerald, D. M., Narbonne, G. M., Pufahl, P. K., and Dalrymple, R. W.: The Mall Bay Formation (Ediacaran) and the protracted onset of the Gaskiers glaciation in Newfoundland, Canada, Precambrian Research, 405, 107369, https://doi.org/10.1016/j.precamres.2024.107369, 2024.

Goddéris, Y., Donnadieu, Y., Dessert, C., Dupré, B., Fluteau, F., François, L. M., Meert, J., Nédélec, A., and Ramstein, G.: Coupled modeling of global carbon cycle and climate in the Neoproterozoic: links between Rodinia breakup and major glaciations, Comptes Rendus Geoscience, 339, 212–222, https://doi.org/10.1016/j.crte.2005.12.002, 2007.

Gómez, N., Lowe, D., Mills, A., Kommescher, S., and Lam, R.: Interplay of Ediacaran glaciation and sediment provenance revealed by detrital zircon U-Pb geochronology and Hf isotope geochemistry in the Bonavista Peninsula (Newfoundland), GSA Bulletin, https://doi.org/10.1130/B38347.1, 2025a.

Gómez, N., Lowe, D., Kommescher, S., and Mills, A.: Unraveling recycling and climate influence on detrital U-Pb geochronology of titanite and apatite: An example from the Gaskiers Glaciation in Newfoundland, Precambrian Research, 427, 107871, https://doi.org/10.1016/j.precamres.2025.107871, 2025b.

Gómez, N., Lowe, D., Mills, A., Slaney, N., and Arnott, R. W. C.: Ediacaran proximal glaciomarine sedimentation in the Bonavista Peninsula, Avalon Zone, Newfoundland, Canada, Journal of Sedimentary Research, 96, 130–157, https://doi.org/10.2110/jsr.2025.022, 2026.

Gough, D. O.: Solar interior structure and luminosity variations, Sol Phys, 74, 21–34, https://doi.org/10.1007/BF00151270, 1981.

Herrington, A. R. and Poulsen, C. J.: Terminating the Last Interglacial: The Role of Ice Sheet–Climate Feedbacks in a GCM Asynchronously Coupled to an Ice Sheet Model, https://doi.org/10.1175/JCLI-D-11-00218.1, 2011.

Hoffman, P. F., Kaufman, A. J., Halverson, G. P., and Schrag, D. P.: A Neoproterozoic Snowball Earth, Science, 281, 1342–1346, https://doi.org/10.1126/science.281.5381.1342, 1998.

Hoffman, P. F., Abbot, D. S., Ashkenazy, Y., Benn, D. I., Brocks, J. J., Cohen, P. A., Cox, G. M., Creveling, J. R., Donnadieu, Y., Erwin, D. H., Fairchild, I. J., Ferreira, D., Goodman, J. C., Halverson, G. P., Jansen, M. F., Le Hir, G., Love, G. D., Macdonald, F. A., Maloof, A. C., Partin, C. A., Ramstein, G., Rose, B. E. J., Rose, C. V., Sadler, P. M., Tziperman, E., Voigt, A., and Warren, S. G.: Snowball Earth climate dynamics and Cryogenian geology-geobiology, Science Advances, 3, e1600983, https://doi.org/10.1126/sciadv.1600983, 2017.

Hourdin, F., Rio, C., Grandpeix, J.-Y., Madeleine, J.-B., Cheruy, F., Rochetin, N., Jam, A., Musat, I., Idelkadi, A., Fairhead, L., Foujols, M.-A., Mellul, L., Traore, A.-K., Dufresne, J.-L., Boucher, O., Lefebvre, M.-P., Millour, E., Vignon, E., Jouhaud, J., Diallo, F. B., Lott, F., Gastineau, G., Caubel, A., Meurdesoif, Y., and Ghattas, J.: LMDZ6A: The Atmospheric Component of the IPSL Climate Model With Improved and Better Tuned Physics, Journal of Advances in Modeling Earth Systems, 12, e2019MS001892, https://doi.org/10.1029/2019MS001892, 2020.

Jacob, R. L.: Low frequency variability in a simulated atmosphere-ocean system, University of Wisconsin - Madison, Madison, USA, 170 pp., 1997.

https://doi.org/10.5194/egusphere-2026-3617
Preprint. Discussion started: 30 June 2026

Judd, E. J., Tierney, J. E., Lunt, D. J., Montañez, I. P., Huber, B. T., Wing, S. L., and Valdes, P. J.: A 485-million-year history of Earth's surface temperature, Science, 385, eadk3705, https://doi.org/10.1126/science.adk3705, 2024.

Kirschvink, J. L.: Late Proterozoic Low-Latitude Global Glaciation: the Snowball Earth, in: The Proterozoic Biosphere: a Multidisciplinary Study, vol. 52, edited by: Schopf, J. W. and Klein, C., Cambridge University Press, New York, USA, 51–52, 1992.

Krinner, G., Viovy, N., de Noblet-Ducoudré, N., Ogée, J., Polcher, J., Friedlingstein, P., Ciais, P., Sitch, S., and Prentice, I. C.: A dynamic global vegetation model for studies of the coupled atmosphere-biosphere system, Global Biogeochemical Cycles, 19, https://doi.org/10.1029/2003GB002199, 2005.

Ladant, J.-B. and Donnadieu, Y.: Palaeogeographic regulation of glacial events during the Cretaceous supergreenhouse, Nat Commun, 7, 12771, https://doi.org/10.1038/ncomms12771, 2016.

Ladant, J.-B., Donnadieu, Y., Lefebvre, V., and Dumas, C.: The respective role of atmospheric carbon dioxide and orbital parameters on ice sheet evolution at the Eocene-Oligocene transition, Paleoceanography, 29, 810–823, https://doi.org/10.1002/2013PA002593, 2014.

Lan, Z., Huyskens, M. H., Ren, R., and Yin, Q.-Z.: A potentially New Early Ediacaran glaciation, J. Earth Sci., 35, 1810–1819, https://doi.org/10.1007/s12583-024-1979-7, 2024.

Laskar, J., Robutel, P., Joutel, F., Gastineau, M., Correia, A. C. M., and Levrard, B.: A long-term numerical solution for the insolation quantities of the Earth, A&A, 428, 261–285, https://doi.org/10.1051/0004-6361:20041335, 2004.

Leloup, G., Quiquet, A., Roche, D. M., Dumas, C., and Paillard, D.: Hysteresis of the Antarctic Ice Sheet With a Coupled Climate-Ice-Sheet Model, Geophysical Research Letters, 52, e2024GL111492, https://doi.org/10.1029/2024GL111492, 2025.

Lenton, T. M., Dahl, T. W., Daines, S. J., Mills, B. J. W., Ozaki, K., Saltzman, M. R., and Porada, P.: Earliest land plants created modern levels of atmospheric oxygen, PNAS, 113, 9704–9709, https://doi.org/10.1073/pnas.1604787113, 2016.

Letsch, D., Large, S. J. E., Buechi, M. W., Winkler, W., and von Quadt, A.: Ediacaran glaciations of the west African Craton – Evidence from Morocco, Precambrian Research, 310, 17–38, https://doi.org/10.1016/j.precamres.2018.02.015, 2018.

Linnemann, U., Pidal, A. P., Hofmann, M., Drost, K., Quesada, C., Gerdes, A., Marko, L., Gärtner, A., Zieger, J., Ulrich, J., Krause, R., Vickers-Rich, P., and Horak, J.: A ~565 Ma old glaciation in the Ediacaran of peri-Gondwanan West Africa, Int J Earth Sci (Geol Rundsch), 107, 885–911, https://doi.org/10.1007/s00531-017-1520-7, 2018.

Linnemann, U., Hofmann, M., Gärtner, A., Gärtner, J., Zieger, J., Krause, R., Haenel, R., Mende, K., Ovtcharova, M., Schaltegger, U., and Vickers-Rich, P.: An Upper Ediacaran Glacial Period in Cadomia: the Granville tillite (Armorican Massif) – sedimentology, geochronology and provenance, Geological Magazine, 159, 999–1013, https://doi.org/10.1017/S0016756821001011, 2022.

Liu, P., Liu, Y., Wang, R., Li, S., Sun, Y., Wen, B., and Shen, B.: Maintenance of the great late Ediacaran ice age, Nat Commun, 16, 3602, https://doi.org/10.1038/s41467-025-58936-7, 2025.

Macdonald, F. A., Swanson-Hysell, N. L., Park, Y., Lisiecki, L., and Jagoutz, O.: Arc-continent collisions in the tropics set Earth's climate state, Science, 364, 181–184, https://doi.org/10.1126/science.aav5300, 2019.

https://doi.org/10.5194/egusphere-2026-3617
Preprint. Discussion started: 30 June 2026

Matthews, J. J., Liu, A. G., Yang, C., McIlroy, D., Levell, B., and Condon, D. J.: A Chronostratigraphic Framework for the Rise of the Ediacaran Macrobiota: New Constraints from Mistaken Point Ecological Reserve, Newfoundland, GSA Bulletin, 133, 612–624, https://doi.org/10.1130/B35646.1, 2021.

Merdith, A. S., Williams, S. E., Collins, A. S., Tetley, M. G., Mulder, J. A., Blades, M. L., Young, A., Armistead, S. E., Cannon, J., Zahirovic, S., and Müller, R. D.: Extending full-plate tectonic models into deep time: Linking the Neoproterozoic and the Phanerozoic, Earth-Science Reviews, 214, 103477, https://doi.org/10.1016/j.earscirev.2020.103477, 2021.

Merdith, A. S., Gernon, T. M., Maffre, P., Donnadieu, Y., Goddéris, Y., Longman, J., Müller, R. D., and Mills, B. J. W.: Phanerozoic icehouse climates as the result of multiple solid-Earth cooling mechanisms, Science Advances, 11, eadm9798, https://doi.org/10.1126/sciadv.adm9798, 2025.

Mills, A. J., Normore, L., Gomez, N., Dunning, G. R., and Lowe, D. G.: A tale of two basins: juxtaposition of the Ediacaran fossil-bearing St. John's Basin against the Ediacaran glaciovolcanic Bonavista Basin on the Bonavista Peninsula, Avalon Zone, Newfoundland, Atlantic Geoscience, 60, 131–150, https://doi.org/10.4138/atlgeo.2024.007, 2024.

Mills, B. J. W., le Hir, G., Merdith, A., Gurung, K., Bowyer, F. T., Krause, A. J., Sanchez-Baracaldo, P., Hunter, S. J., and Zhang, Y.: Exploring Neoproterozoic climate and biogeochemical evolution in the SCION model, Global and Planetary Change, 249, 104791, https://doi.org/10.1016/j.gloplacha.2025.104791, 2025.

Minguez, D., Kodama, K. P., and Hillhouse, J. W.: Paleomagnetic and cyclostratigraphic constraints on the synchroneity and duration of the Shuram carbon isotope excursion, Johnnie Formation, Death Valley Region, CA, Precambrian Research, 266, 395–408, https://doi.org/10.1016/j.precamres.2015.05.033, 2015.

Mlawer, E. J., Taubman, S. J., Brown, P. D., Iacono, M. J., and Clough, S. A.: Radiative transfer for inhomogeneous atmospheres: RRTM, a validated correlated-k model for the longwave, Journal of Geophysical Research: Atmospheres, 102, 16663–16682, https://doi.org/10.1029/97JD00237, 1997.

Mulder, J. A., Everard, J. L., Cumming, G., Meffre, S., Bottrill, R. S., Merdith, A. S., Halpin, J. A., McNeill, A. W., and Cawood, P. A.: Neoproterozoic opening of the Pacific Ocean recorded by multi-stage rifting in Tasmania, Australia, Earth-Science Reviews, 201, 103041, https://doi.org/10.1016/j.earscirev.2019.103041, 2020.

Niu, Y., Shi, G. R., Zhang, Q., Jones, B. G., Wang, X., and Zhao, G.: Ediacaran Cordilleran-type mountain ice sheets and their erosion effects, Earth-Science Reviews, 249, 104671, https://doi.org/10.1016/j.earscirev.2023.104671, 2024.

d'Orgeval, T., Polcher, J., and de Rosnay, P.: Sensitivity of the West African hydrological cycle in ORCHIDEE to infiltration processes, Hydrology and Earth System Sciences, 12, 1387–1401, https://doi.org/10.5194/hess-12-1387-2008, 2008.

Pecoits, E., Gingras, M. K., and Konhauser, K. O.: Chapter 53 Las Ventanas and San Carlos formations, Maldonado Group, Uruguay, Geological Society, London, Memoirs, 36, 555–564, https://doi.org/10.1144/M36.53, 2011.

Pohl, A., Donnadieu, Y., Le Hir, G., Buoncristiani, J.-F., and Vennin, E.: Effect of the Ordovician paleogeography on the (in)stability of the climate, Clim. Past, 10, 2053–2066, https://doi.org/10.5194/cp-10-2053-2014, 2014.

Pohl, A., Donnadieu, Y., Le Hir, G., Ladant, J.-B., Dumas, C., Alvarez-Solas, J., and Vandenbroucke, T. R. A.: Glacial onset predated Late Ordovician climate cooling, Paleoceanography, 31, 800–821, https://doi.org/10.1002/2016PA002928, 2016a.

Pohl, A., Nardin, E., Vandenbroucke, T. R. A., and Donnadieu, Y.: High dependence of Ordovician ocean surface circulation on atmospheric CO2 levels, Palaeogeography, Palaeoclimatology, Palaeoecology, 458, 39–51, https://doi.org/10.1016/j.palaeo.2015.09.036, 2016b.

https://doi.org/10.5194/egusphere-2026-3617
Preprint. Discussion started: 30 June 2026

Powers, M. C.: A new roundness scale for sedimentary particles, Journal of Sedimentary Research, 23, 117–119, https://doi.org/10.1306/D4269567-2B26-11D7-8648000102C1865D, 1953.

Pu, J. P., Bowring, S. A., Ramezani, J., Myrow, P., Raub, T. D., Landing, E., Mills, A., Hodgin, E., and Macdonald, F. A.: Dodging snowballs: Geochronology of the Gaskiers glaciation and the first appearance of the Ediacaran biota, Geology, 44, 955–958, https://doi.org/10.1130/G38284.1, 2016.

Quiquet, A., Dumas, C., Ritz, C., Peyaud, V., and Roche, D. M.: The GRISLI ice sheet model (version 2.0): calibration and validation for multi-millennial changes of the Antarctic ice sheet, Geoscientific Model Development, 11, 5003–5025, https://doi.org/10.5194/gmd-11-5003-2018, 2018.

Quiquet, A., Dumas, C., Paillard, D., Ramstein, G., Ritz, C., and Roche, D. M.: Deglacial Ice Sheet Instabilities Induced by Proglacial Lakes, Geophysical Research Letters, 48, e2020GL092141, https://doi.org/10.1029/2020GL092141, 2021.

Retallack, G. J.: Towards a glacial subdivision of the Ediacaran Period, with an example of the Boston Bay Group, Massachusetts, Australian Journal of Earth Sciences, 69, 223–250, https://doi.org/10.1080/08120099.2021.1954088, 2022.

Ritz, C., Rommelaere, V., and Dumas, C.: Modeling the evolution of Antarctic ice sheet over the last 420,000 years: Implications for altitude changes in the Vostok region, Journal of Geophysical Research: Atmospheres, 106, 31943–31964, https://doi.org/10.1029/2001JD900232, 2001.

Rooney, A. D., Cantine, M. D., Bergmann, K. D., Gómez-Pérez, I., Al Baloushi, B., Boag, T. H., Busch, J. F., Sperling, E. A., and Strauss, J. V.: Calibrating the coevolution of Ediacaran life and environment, Proceedings of the National Academy of Sciences, 117, 16824–16830, https://doi.org/10.1073/pnas.2002918117, 2020.

Scotese, C. R.: PALEOMAP PaleoAtlas for GPlates and the PaleoData Plotter Program, PALEOMAP Project, 2016.

Scotese, C. R. and Wright, N.: PALEOMAP paleodigital elevation models (PaleoDEMS) for the Phanerozoic, PALEOMAP Proj, 2018.

Scotese, C. R., Song, H., Mills, B. J. W., and van der Meer, D. G.: Phanerozoic paleotemperatures: The earth's changing climate during the last 540 million years, Earth-Science Reviews, 215, 103503, https://doi.org/10.1016/j.earscirev.2021.103503, 2021.

Shields, G. A., Mills, B. J. W., Zhu, M., Raub, T. D., Daines, S. J., and Lenton, T. M.: Unique Neoproterozoic carbon isotope excursions sustained by coupled evaporite dissolution and pyrite burial, Nat. Geosci., 12, 823–827, https://doi.org/10.1038/s41561-019-0434-3, 2019.

Środoń, J., Condon, D. J., Golubkova, E., Millar, I. L., Kuzmenkova, O., Paszkowski, M., Mazur, S., Kędzior, A., Drygant, D., Ciobotaru, V., and Liivamägi, S.: Ages of the Ediacaran Volyn-Brest trap volcanism, glaciations, paleosols, Podillya Ediacaran soft-bodied organisms, and the Redkino-Kotlin boundary (East European Craton) constrained by zircon single grain U-Pb dating, Precambrian Research, 386, 106962, https://doi.org/10.1016/j.precamres.2023.106962, 2023.

Tan, M., Li, Z., Lan, Z., An, W., and Wang, D.: Rodinia supercontinent assembly in the southeastern North China Craton: Detrital zircon evidence from the late Ediacaran Fengtai Formation, Precambrian Research, 422, 107775, https://doi.org/10.1016/j.precamres.2025.107775, 2025.

Tasistro-Hart, A. R., Macdonald, F. A., Crowley, J. L., and Schmitz, M. D.: Four-million-year Marinoan snowball shows multiple routes to deglaciation, Proceedings of the National Academy of Sciences, 122, e2418281122, https://doi.org/10.1073/pnas.2418281122, 2025.

https://doi.org/10.5194/egusphere-2026-3617
Preprint. Discussion started: 30 June 2026

Thompson, M. D. and Bowring, S. A.: Age of the Squantum "tillite," Boston Basin, Massachusetts; U-Pb zircon constraints on terminal Neoproterozoic glaciation, American Journal of Science, 300, 630–655, https://doi.org/10.2475/ajs.300.8.630, 2000.

Tindal, B.: Geological constraints on Neoproterozoic glacial episodes, PhD, University of Cambridge, Cambridge, UK, 275 pp., https://doi.org/10.17863/CAM.93553, 2023.

Umbgrove, J. H. F.: The Pulse of the Earth, Springer Netherlands, Dordrecht, 358 pp., https://doi.org/10.1007/978-94-017-5902-1, 1947.

Wang, R., Shen, B., Lang, X., Wen, B., Mitchell, R. N., Ma, H., Yin, Z., Peng, Y., Liu, Y., and Zhou, C.: A Great late Ediacaran ice age, National Science Review, nwad117, https://doi.org/10.1093/nsr/nwad117, 2023a.

Wang, R., Yin, Z., and Shen, B.: A late Ediacaran ice age: The key node in the Earth system evolution, Earth-Science Reviews, 247, 104610, https://doi.org/10.1016/j.earscirev.2023.104610, 2023b.

Wang, X., Zhang, X., and Liu, W.: Biostratigraphic constraints on the age of Neoproterozoic glaciation in North China, Journal of Asian Earth Sciences, 219, 104894, https://doi.org/10.1016/j.jseaes.2021.104894, 2021.

Wen, B., Luo, C., Li, Y.-X., and Lin, Y.: Late Ediacaran inertial-interchange true polar wander (IITPW) event: a new road to reconcile the enigmatic paleogeography prior to the final assembly of Gondwana, Turkish Journal of Earth Sciences, 31, 425–437, https://doi.org/10.55730/1300-0985.1811, 2022.

Westerhold, T., Marwan, N., Drury, A. J., Liebrand, D., Agnini, C., Anagnostou, E., Barnet, J. S. K., Bohaty, S. M., Vleeschouwer, D. D., Florindo, F., Frederichs, T., Hodell, D. A., Holbourn, A. E., Kroon, D., Lauretano, V., Littler, K., Lourens, L. J., Lyle, M., Pälike, H., Röhl, U., Tian, J., Wilkens, R. H., Wilson, P. A., and Zachos, J. C.: An astronomically dated record of Earth's climate and its predictability over the last 66 million years, Science, 369, 1383–1387, https://doi.org/10.1126/science.aba6853, 2020.

Willeit, M., Ganopolski, A., Robinson, A., and Edwards, N. R.: The Earth system model CLIMBER-X v1.0 – Part 1: Climate model description and validation, Geoscientific Model Development, 15, 5905–5948, https://doi.org/10.5194/gmd-15-5905-2022, 2022.

Wong Hearing, T. W., Pohl, A., Williams, M., Donnadieu, Y., Harvey, T. H. P., Scotese, C. R., Sepulchre, P., Franc, A., and Vandenbroucke, T. R. A.: Quantitative comparison of geological data and model simulations constrains early Cambrian geography and climate, Nat Commun, 12, 3868, https://doi.org/10.1038/s41467-021-24141-5, 2021.

Wong Hearing, T. W., Tindal, B. H., Vandyk, T. M., Na, L., Pohl, A., Liu, A. G., Harvey, T. H. P., and Williams, M.: Ediacaran coupling of climate and biosphere dynamics, GSA Bulletin, accepted, 2026.

Xiao, S., Bao, H., Wang, H., Kaufman, A. J., Zhou, C., Li, G., Yuan, X., and Ling, H.: The Neoproterozoic Quruqtagh Group in eastern Chinese Tianshan: evidence for a post-Marinoan glaciation, Precambrian Research, 130, 1–26, https://doi.org/10.1016/j.precamres.2003.10.013, 2004.

Xiao, S. H. and Narbonne, G. M.: Chapter 18 - The Ediacaran Period, in: Geologic Time Scale 2020, edited by: Gradstein, F. M., Ogg, J. G., Schmitz, M. D., and Ogg, G. M., Elsevier, 521–561, https://doi.org/10.1016/B978-0-12-824360-2.00018-8, 2020.

Yang, C., Rooney, A. D., Condon, D. J., Li, X.-H., Grazhdankin, D. V., Bowyer, F. T., Hu, C., Macdonald, F. A., and Zhu, M.: The tempo of Ediacaran evolution, Science Advances, 7, eabi9643, https://doi.org/10.1126/sciadv.abi9643, 2021.

https://doi.org/10.5194/egusphere-2026-3617
Preprint. Discussion started: 30 June 2026

Youbi, N., Ernst, R. E., Söderlund, U., Boumehdi, M. A., Lahna, A. A., Tassinari, C. C. G., Moume, W. E., and Bensalah, M. K.: The Central Iapetus magmatic province: An updated review and link with the ca. 580 Ma Gaskiers glaciation, in: Mass Extinctions, Volcanism, and Impacts: New Developments, edited by: Adatte, T., Bond, D. P. G., and Keller, G., Geological Society of America, 0, https://doi.org/10.1130/2020.2544(02), 2020.

Yuan, X., Chen, Z., Xiao, S., Zhou, C., and Hua, H.: An early Ediacaran assemblage of macroscopic and morphologically differentiated eukaryotes, Nature, 470, 390–393, https://doi.org/10.1038/nature09810, 2011.

Yue, L., Ji, Y., Chu, Z., Zhang, C., Cui, Y., Vandeginste, V., Zong, Y., and Yan, G.: Ediacaran glaciogenic deposits within a carbonate platform background: insights from the Fengtai formation in the southeastern margin of the North China Craton, Geosci J, 29, 342–361, https://doi.org/10.1007/s12303-025-00034-3, 2025.